

COMPARTMENT FIRE-GENERATED ENVIRONMENT AND SMOKE FILLING

Leonard Y. Cooper

FIRE SAFETY OF BUILDING DESIGNS

Introduction

The following generic problem must be solved if one is to be able to establish the fire safety of building designs:

- Given:** Initiation of a fire in a compartment or enclosed space.
- Predict:** The environment that develops at likely locations of occupancy, at likely locations of fire/smoke sensor hardware (e.g., detectors and sprinkler links), and in locations of safe refuge and along likely egress paths.
- Compute:** The time of fire/smoke sensor hardware response and the time of onset of conditions untenable to life and/or property. This computation would be carried out from the above predictions, using known response characteristics of people, hardware, and materials.

The above is only a simple sketch of the overall problem that is likely to be associated with the interesting details of many real fire scenarios. A long-term challenge of fire science and technology is to solve the above type of problem, even when it is formulated in elaborate detail. Compartment fire modeling is the branch of fire science and technology which develops the necessary tools to address this generic problem.

This chapter will describe some of the key phenomena that occur in compartment fires, and it will focus on smoke filling which is one of the simplest quantitative global descriptions of these phenomena. A specific smoke-filling model will be presented, and solutions to its model equations will be discussed along with example applications.

Dr. Leonard Y. Cooper is a Research Engineer in the Building and Fire Research Laboratory of the National Institute of Standards and Technology. Since 1978 his research has focused on the development of mathematical models of fire phenomena and on the assembly of these into compartment fire models and associated computer programs for practical and research-oriented compartment fire simulations.

Compartment Fire-Generated Environment

Figures 3-10.1 through 3-10.8 depict the various phenomena that make up the compartment fire-generated environment to be predicted when compartment fire modeling is adopted. These figures are intended to illustrate the representative conditions at different instants of time in two generic compartment spaces: (1) an almost-fully enclosed single-room compartment of fire origin and (2) an almost-fully enclosed, freely connected, two-room compartment made up of the room of fire origin and an adjacent space. A description of the phenomena depicted in these figures follows. The physical bases of assumption that can be used to simplify descriptions of some of these phenomena are included in the discussion. Some of these will be important in placing the simple smoke-filling model into the perspective of the overall complex dynamic fire environment.

Room of Fire Involvement

Fire growth in the combustible of fire origin: An unwanted ignition leading rapidly to flaming is assumed to occur within an enclosed space. This ignition is depicted in Figure 3-10.1 as occurring on the cushion of a couch in, say, a residential type of occupancy. It is, however, important to realize that all of the discussion to follow, and Figure 3-10.1 itself, is also relevant to fire scenarios which may develop in other kinds of occupancies, e.g., as a result of ignitions in stacked commodity warehouse enclosures, places of assembly, etc.

Within a few seconds of ignition, early flame spread quickly leads to a flaming fire with a power output of the order of a few tens of kW (a power level characteristic of a small wastepaper basket fire). The fire continues to grow. Besides releasing energy, the combustion process also yields a variety of other products, including toxic and nontoxic gases and solids. Together, all of these products are referred to as the "smoke" produced by the fire.

With an adequate description of the ignition source and the involved combustible (e.g., ignited paper match on the corner of a couch whose frame, cushioning and finishing materials, and construction were well defined), one would hope that fire science and technology would provide methods to predict the fire spread and growth process from onset of ignition. Toward this end, ongoing research on flame

spread and combustion is under way in a variety of fire research institutions throughout the world. (Examples of such research include boundary layer analyses and experiments with flame spread on idealized materials and geometries; and flame spread tests and rate of heat release tests on small samples of real material composites.) However, for the present and the foreseeable future, it is beyond the state-of-the-art of fire technology to make the required fire growth prediction with any generality. This situation leads to a dilemma for the modeler of compartment fire environments, because the physical and chemical mechanisms which govern the dynamics of the combustion zone actually drive the basic intra-compartment smoke migration phenomena whose simulations are being sought.

A practical engineering solution to the above dilemma, proposed and supported by Cooper,^{1,2} lies in the following compromise in simulation accuracy:

Prior to the time of potential flashover, it is reasonable to neglect the effect of the enclosure on flame spread and to assume that, from the time of ignition to the time shortly before potential flashover, the combustion zone in a particular grouping of combustibles develops as it would in a free-burn situation.

[Free burn here is defined as a burn of the combustibles in a large (compared to the combustion zone), ventilated space with relatively quiescent atmosphere.] To implement these ideas, one simply uses empirical, free-burn test data (which may or may not be presently available) to describe the combustion physics of a fire whose hazard is being evaluated. This compromise would, in the course of time, be supplanted by analytic models of flame spread and fire growth to the extent the future results of research lead to satisfactory methods for predicting such phenomena.

The implementation of the above compromise is, in principle, relatively simple. But for general use, it must be supported by an extensive data base acquired from a series of actual full-scale free-burn tests. This kind of data is being acquired with some regularity at fire test laboratories such as those of the National Institute of Standards and Technology and the Factory Mutual Research Corporation.^{3,4,5}

Development of the plume: As depicted in Figure 3-10.2, a large fraction, λ_r , of the rate of energy released in the high-temperature combustion zone is transferred away by radiation. The transferred energy, $\lambda_r \dot{Q}(t)$, irradiates nearby surfaces of the combustible and faraway wall, ceiling, etc., surfaces which are in the line-of-sight of the combustion zone. The actual value of λ_r associated with the free-burn of a specific array of combustibles is often deduced from data acquired during the aforementioned type of free-burn tests. For typical hazardous flaming fires, λ_r is usually of the order of 0.35.

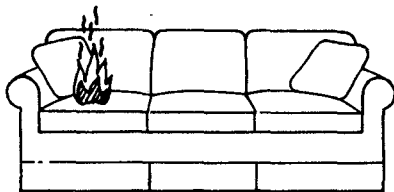


Fig. 3-10.1. Events immediately after ignition.

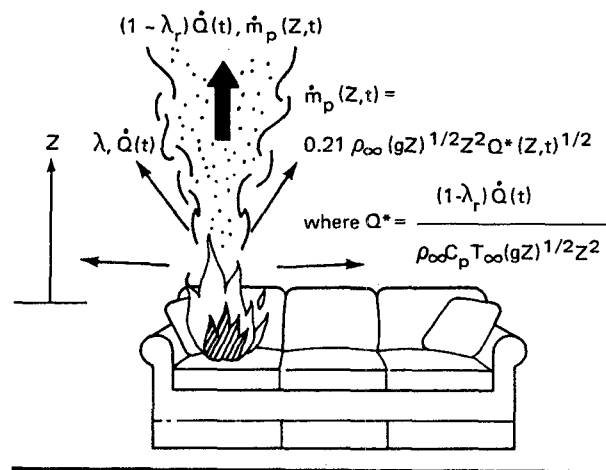


Fig. 3-10.2. Development of the plume.

Because of the elevated temperature of the products of combustion, buoyancy forces drive them out of the growing combustion zone and up toward the ceiling. In this way, a plume of upward-moving elevated-temperature gases and particulates is formed above the fire. For the full height of the plume and at its periphery, relatively quiescent and cool gases are entrained laterally and mixed with the plume as it continues its ascent to the ceiling. As a result of this entrainment, the total mass flow in the plume continuously increases, and the average temperature and average concentration of products of combustion in the plume continuously decrease with increasing height. With reasonable accuracy, the plume dynamics at any instant of time can be quantitatively described as a function of the rate of energy, $(1 - \lambda_r)\dot{Q}(t)$, convected up from the combustion zone. A description of the concentration of combustion products in the plume would require, in addition, the combustion zone's rate of product generation. With regard to predictions of the dynamics of the plume, results can be provided at a variety of different levels of detail.^{6,7,8} For example, Zukoski *et al* provide the formula in Figure 3-10.2 as an estimate of the mass flux in the plume, \dot{m}_p , at a distance Z above the combustion zone.⁷

Plume-ceiling interaction: As depicted in Figure 3-10.3, when the hot plume gases impinge on the ceiling, they spread across it forming a relatively thin radial jet. This jet of hot gases contains all of the smoke generated from the combustion zone, and all the ambient air which was entrained along the length of the plume.

As the hot jet moves outward under the ceiling surface, it entrains ambient air from below. It transfers energy by conduction to the relatively cool adjacent ceiling surface, and by convection to the entrained air. It is retarded by frictional forces from the ceiling surface above, and by turbulent momentum transfer to the entrained air from below. As a result of all this flow and heat transfer activity, the ceiling jet continuously decreases in temperature, smoke concentration, and velocity, and increases in thickness with increasing radius.

Research reported in the literature has led to results for predicting the quantitative aspects of ceiling-jet dynamics that can be used for selecting and locating smoke detectors and

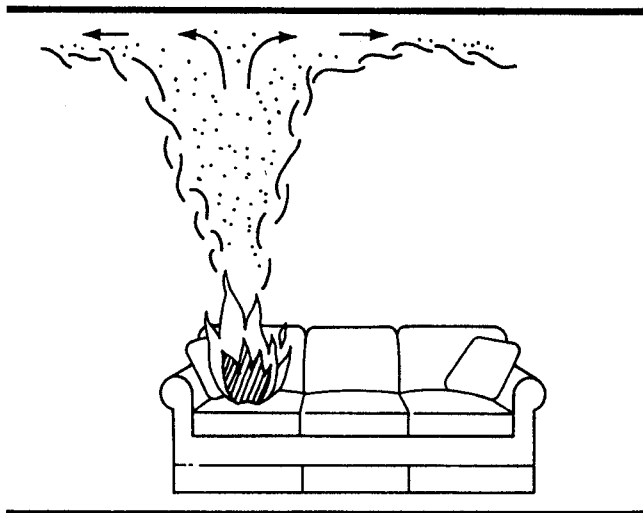


Fig. 3-10.3. The plume-ceiling interaction.

fusible link sprinkler head actuators, and for the mathematical modeling of overall compartment fire environments.⁹⁻¹⁸

With regard to detectors and fusible links, knowledge of the properties of the ceiling jet is the key to the prediction of the response of properly deployed devices in real fire scenarios. With regard to the overall modeling of compartment fire environments, the basic information that must be extracted from the ceiling-jet properties is the rate of heat transfer to the ceiling surface. Experiments have shown that this heat transfer can be significant, of the order of several tens of percent of the total energy released by the combustion zone, and, as a result, it is key to predicting the temperature of the smoke which ultimately spreads throughout the enclosure. Also, a reasonable estimate of this rate of heat transfer is required for estimating temperatures of the ceiling surface material itself.

Ceiling jet-wall interaction: The ceiling jet continues to move radially outward under the ceiling surface, and it eventually reaches the bounding walls of the enclosure. As depicted in Figure 3-10.4, the ceiling jet (now somewhat reduced in temperature from its highest levels near the plume) impinges and turns downward at the ceiling-wall juncture, thereby initiating a downward-directed wall jet.

The downward wall jet is of higher temperature and lower density than the ambient air into which it is being driven. The jet is, therefore, retarded by buoyancy in its downward descent, and at some distance below the ceiling the downward motion of the smoky jet is eventually halted. The wall jet is also retarded (probably to a lesser degree) by frictional forces at the wall surface, and it is cooled by conductive/convective heat transfer to relatively cool wall surfaces. Momentum and heat transfer from the jet occur away from the wall as the jet's outer flow is sheared off and driven back upward on account of buoyancy. In its turn, the now upward-moving flow entrains ambient air in a manner which is reminiscent of entrainment into the original fire plume. Eventually a relatively quiescent upper gas layer is formed below the continuing ceiling-jet flow activity.

The strength of the wall-jet flow activity will be determined by the characteristics of the ceiling jet at the position of its impingement with the wall. For fire scenarios where the proximity of the walls to the fire is no greater than a room

height or so, it is reasonable to speculate that, based on test results,^{19,20} rates of conductive/convective heat transfer to wall surfaces can be significant, of the order of tens of percent of the fire's energy release, and that entrainment to the upward moving, reverse portion of the wall flow can lead to significant variations of the early rate of thickening of the upper gas layer. On the other hand, if walls are several room heights from the fire, then it is possible that the ceiling jet will be relatively weak by the time it reaches the walls, in the sense that ceiling jet-wall interactions may not play an important role in the dynamics of the overall fire environment.

Besides being important in the prediction of the overall fire environment, knowledge of the flow and temperature environments local to vigorous ceiling jet-wall interaction zones would be the key to predicting the response of wall-mounted smoke detectors, fusible links, etc.

Development and growth of the upper layer—"smoke filling": The gases in the ceiling and wall jets redistribute themselves across the upper volume of the room. Eventually, a relatively quiescent, elevated temperature upper smoke layer of uniform thickness is formed below the continuing ceiling-jet flow activity. As the thickness of this layer grows, it eventually submerges the flows generated by the ceiling jet-wall interactions. The bottom of the layer is defined by a distinctive material interface which separates the lower ambient air from the upper, heated, smoke-laden gases. With increasing time the level of the smoke layer interface continues to drop, and the temperature and smoke concentration of the upper layer continue to rise.

In general, one would hope that fire detection, successful occupant alarm, and, if appropriate, successful intervention hardware response would occur during the state of fire growth described above. As suggested earlier, rationally engineered design in this regard would be possible with predictions of the dynamic fire environments local to deployed devices, and with predictions of the resulting response of such devices.

For reasons, already mentioned, some detail in the description of plume, ceiling-jet, and ceiling jet-wall flow dynamics is required. However, for the purpose of understanding the impact of the overall fire environment on life and property safety, simplified descriptions compatible with the

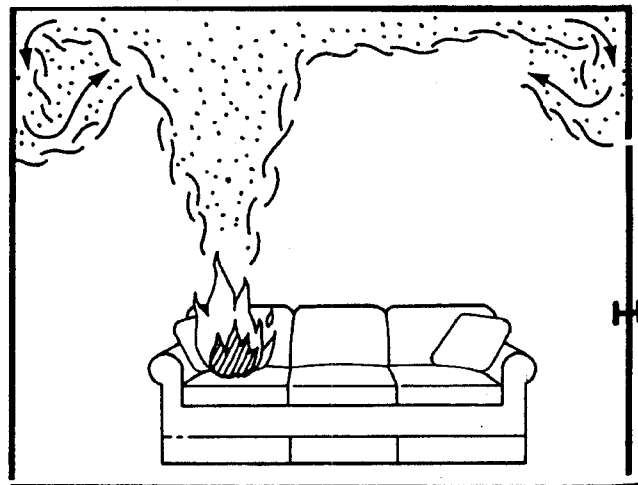


Fig. 3-10.4. Ceiling jet-wall interaction.

aforementioned detail would suffice and, for a variety of practical reasons, would actually be preferable. For this reason, available predictive models of compartment fire environments commonly describe the bulk of upper layer environment in terms of its spatially averaged properties. Thus, at any instant of time, it is typically assumed that the portion of the room which contains the fire-generated products of combustion, i.e., the smoke, is confined to an upper layer of the room. This upper layer is described as having changing thickness and changing, but spatially uniform, temperature and concentration of combustion products. Actual full-scale testing of compartment fire environments has indicated that such a simple means of describing the distribution of products of combustion represents a reasonable compromise between accuracy in simulation and practicability in implementation.

Figure 3-10.5 is a generic depiction of the compartment fire environment at the stage of fire development under discussion. At this stage, whether or not the space of fire involvement is fully enclosed (i.e., all doors and windows are closed and only limited leakage occurs at bounding partitions) or is freely communicating with adjacent space(s) (e.g., open or broken windows, open doors to the outside environment or to an adjacent enclosed space of limited or virtually unlimited extent) becomes very important in the subsequent development of the fire environment. In the sense that the upper layer thickness and temperature would grow most rapidly, the fully enclosed space with most leakage near the floor would lead to the most rapid development of potentially life and property threatening conditions.

Referring again to the depiction in Figure 3-10.5, the fire plume below the smoke layer interface continues to entrain air as it rises to the ceiling. However, as the hot plume gases penetrate the layer interface and continue their ascent, additional entrainment is from an elevated temperature, smoke-laden environment. Also, once the plume gases enter the smoke layer, they are less buoyant relative to this layer than they were relative to the cool lower layer of ambient air. Thus, the continued ascent of plume gases is less vigorous than it would otherwise be in the absence of the upper layer.

The new and more complex two-layer state of the enclosure environment requires that some modification of the

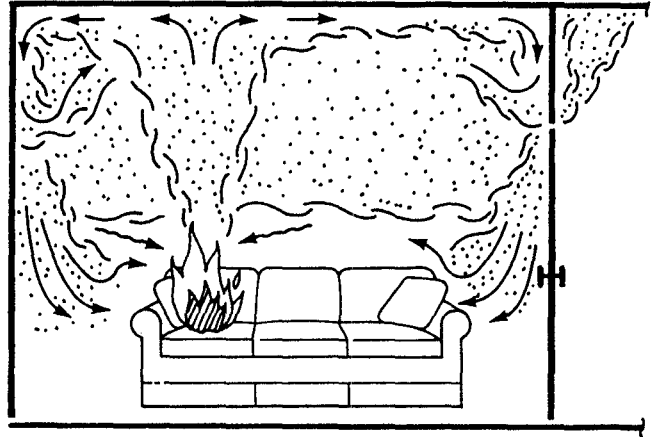


Fig. 3-10.6. Further "smoke filling."

earlier referenced quantitative descriptions of the plume, ceiling-jet, and ceiling jet-wall flow dynamics be introduced. Modifications along these lines are proposed by Cooper.^{21,22}

As depicted in Figure 3-10.6, potentially significant wall flow can develop during the descent of the layer interface. This flow is expected to occur away from regions of vigorous ceiling jet-wall interactions. It is distinct from the previously described upper wall jet and develops because of relatively cool upper wall surfaces which bound the elevated-temperature upper smoke layer. The smoke which is adjacent to these wall surfaces is relatively cool and, therefore, more dense than its surroundings. As a result of this density difference, a continuous, downward-directed wall flow develops which is injected at the smoke interface into the lower, relatively smoke-free layer. Once in the lower layer, the smoke-laden wall flow, now of higher temperature than its surroundings, will be buoyed back upward to either mix with and contaminate the lower layer or to entrain additional (i.e., in addition to the fire plume) lower layer air into the upper layer.

It is noteworthy that the wall effect just described has been observed in full- and reduced-scale fire tests, and that it appears to be particularly significant in enclosures with relatively large ratios of perimeter-to-ceiling height (e.g., in corridors).²³

As a result of its elevated temperature, the smoky upper layer transfers energy by radiation to the ceiling and upper wall surfaces which contain it. As depicted in Figures 3-10.4 and 3-10.5 by the downward-directed arrows, the layer also radiates to the lower surfaces of the enclosure and its contents. Initially, the only significant role of this downward radiation is its effect on human tissue. Indeed, only for downward-directed radiation fluxes significantly in excess of life-threatening levels (characterized by smoke layer temperature levels of the order of 200°C, or by flux levels of the order of 2.5 kW/m²) would the radiant energy feedback to enclosure surfaces and combustibles have a significant impact on fire growth and spread, and on the overall fire environment.^{1,24}

Once radiation feedback becomes of general significance, e.g., when the average upper layer temperature reaches 300 to 400°C, it is likely that the potential for flash-over will develop within a relatively short time interval (compared to the time interval between ignition and the

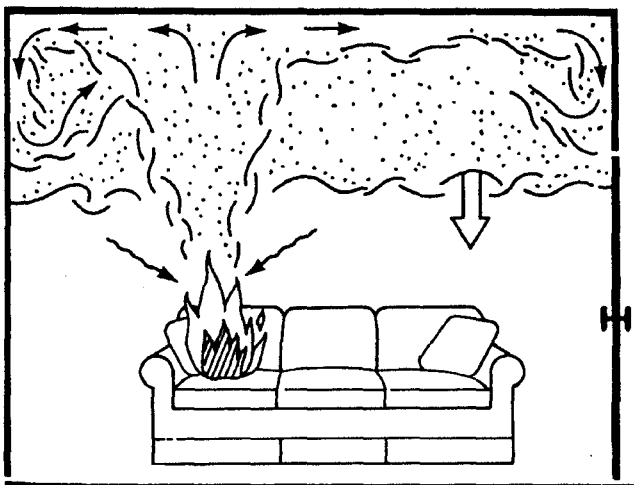


Fig. 3-10.5. Fully enclosed space with developed growing upper layer.



Fig. 3-10.7. Smoke and fresh air exchange between a room of fire involvement and an adjacent space.

onset of a life-threatening environment). The events which develop during this time interval will be referred to here as the "transition stage" of fire development.

The onset of life-threatening conditions, which could be caused by any one of a number of reasons, would occur prior to the transition stage of fire development. Before this event can be predicted, quantitative criteria defining a "life-threatening environment" must be established. These criteria must be defined in terms of those physical parameters for which predictive models of compartment fire environments can provide reasonable estimates. Consistent with the earlier discussion, such parameters include the smoke layer thickness (or vertical position of its interface) and temperature. The concentration of potentially hazardous components of the smoke in the upper layer would also be of basic importance. Criteria for the onset of a life-threatening environment could, for example, be based on the following consideration (which would neglect the effect of lower layer contamination due to wall flows):

When the smoke layer interface is above some specified, characteristic face-elevation, an untenable environment would occur if and when a hazardous radiation exposure from the upper layer is attained. Such an exposure could be defined by a specified upper layer critical temperature. If the interface is below face-elevation, then untenability would occur if and when a second critical smoke layer temperature is attained. However, the latter temperature would be lower than the former one, and untenable conditions would result from burns or the inhalation of hot gases. Once the interface dropped below face elevation, untenability would also occur if and when a specified critical concentration (or a specified exposure dosage) of some hazardous product of combustion was attained.²

Transition stage of fire development: Any detailed analysis and prediction of the fire environment during the transition stage of fire development must, of necessity, take account of the effects of upper layer and upper surface reradiation, in general, and of the complex effects of radiation-enhanced fire growth, in particular. Such an analysis would require a mathematical model of compartment fire phenom-

ena which would be significantly more sophisticated than that which would be required to predict the fire environment prior to, and possibly even following, the transition stage.

Regarding the potential difficulty, uncertainty, inconvenience, and/or cost of carrying out transition stage analysis, it is noteworthy that conservative designs for life and property safety may be possible by implementing a strategy of fire environment analysis which avoided the details of the transition stage entirely. This is done by conservatively assuming that the relatively brief time interval associated with the transition stage shrinks to a flashover jump condition at a relatively early time in the fire scenario.¹

Smoke Spread from the Room of Fire Involvement to Adjacent Spaces

Smoke and fresh air exchange between a room of fire involvement and an adjacent space: Under this and the following subheading, smoke spread phenomena associated with a fire-involved room and a communicating adjacent space will be discussed. Reference here will be made to a fully enclosed, two-room space with relatively large common penetrations (e.g., open doors or windows) through which smoke and ambient air exchange will be so significant as to render inadequate an analysis which treats the room of fire involvement as an isolated enclosure. Regarding the two-room spatial configuration, Figures 3-10.1 through 3-10.5 are still relevant to the early development of conditions within the fire room. As the smoke layer interface drops to the level of the soffit of the communicating doorway(s) or window(s), significant amounts of smoke start to move into the adjacent space from above, while significant amounts of ambient air are driven out of the adjacent space (and into the fire room) from below. From that time on, as depicted in Figure 3-10.7, an interdependent smoke-filling process in each of the two spaces is initiated, and the adjacent space starts to develop a two-layer type of environment.

Throughout the course of typical real-fire scenarios, changes in the absolute pressures of facility spaces are, at the most, of the order of one percent. Yet, dynamic elevation-dependent pressure differences that exist between the rooms

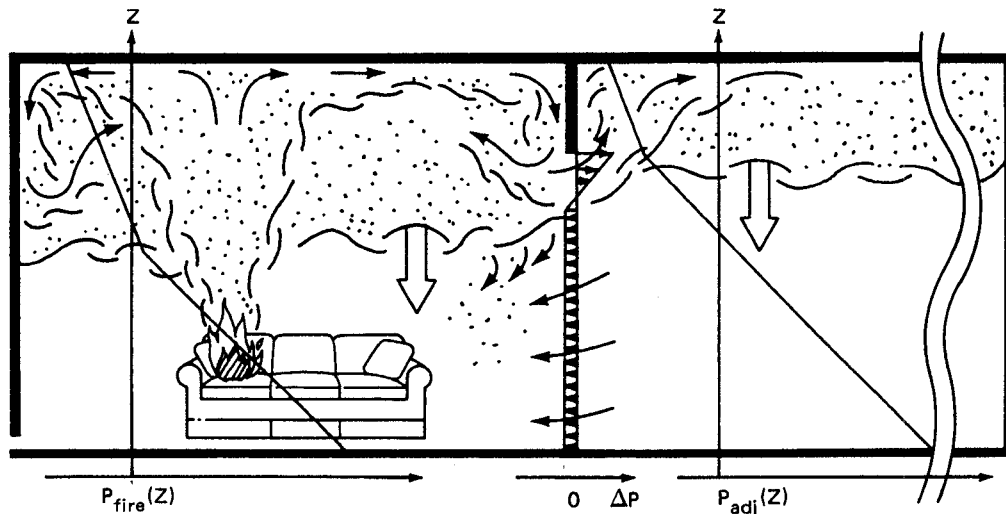


Fig. 3-10.8. Figure 3-10.7 with sketches of pressure distributions.

of fire involvement and adjacent spaces are large enough to drive a significant cross-door exchange of smoke and ambient air.

Toward the left side of Figure 3-10.8 is a sketch of the vertical static pressure distribution, $P_{fire}(Z)$, of the room of fire involvement. This is the pressure distribution that is measured in the bulk of the relatively quiescent-environment room, away from vigorous door and plume flows. Notice that the rate of change of pressure with elevation is uniform and relatively large between the floor and the smoke interface, and is uniform and relatively small within the smoke layer. The reason for this is that the temperature-dependent density throughout each of the two layers is assumed to be uniform, and the lower layer is more dense (i.e., of lower temperature) than the upper one. The pressure at the floor is designated as $P_{fire}(Z = 0) = P_{fire,0}$.

Toward the right side of Figure 3-10.8 is a sketch of the vertical static pressure, $P_{adj}(Z)$, in the adjacent space. There, the change of slope occurs at the elevation of the adjacent space's smoke interface, which is above the smoke interface in the fire room. Also, the slope of the pressure distribution above the interface is consistent with a smoke layer somewhat more dense or cooler than the smoke layer in the fire room. Finally, the pressure at the floor is designated as $P_{adj}(Z) = P_{adj,0}$. The two pressure distributions can be compared by the plot of the pressure difference, $\Delta P(Z) = P_{fire}(Z) - P_{adj}(Z)$, which is sketched in the doorway of Figure 3-10.8. At Z elevations below the soffit where ΔP is positive, gases are driven from the fire room into the adjacent space. At elevations where ΔP is negative, gases are driven from the adjacent space into the fire room. At the unique elevation, called the neutral plane, where ΔP is zero, the gases tend to remain stagnant in both spaces. This is the elevation in the doorway which divides outgoing fire room smoke above from inflowing adjacent space air below.

At any given elevation, it is typical in the modeling of fire-generated doorway/window flows to use Bernoulli's equation to estimate the velocity, $V(Z)$, of the flow coming out of or into the fire room. The flow is assumed to be accelerated from rest to a dynamic pressure, $\rho V^2(Z)/2 = \Delta P(Z)$, where ρ is the density of the gas from which the streamlines originate. Also, at any elevation, the flow is as-

sumed to be constricted at the *vena contracta* of the inlet/outlet jet, as with an orifice, to a fraction, C , of the width $W(Z)$ of the doorway. Then the total rate of mass flow across the doorway per unit height at any elevation would be

$$\rho C V(Z) W(Z) = C W(Z) \sqrt{2\rho \Delta P(Z)}$$

Imposing conservation principles at any instant of time when the layer thicknesses and densities (temperatures) in the two rooms are known, leads to the instantaneous values of $\Delta P(Z = 0)$ and neutral plane elevation.

An in-depth presentation of results for calculating total inlet and outlet mass flows and for general application of the above considerations is presented by Zukoski and Kubota.²⁵ Results on most appropriate values to use for C have been obtained from full-scale fire experiments.²⁶

Door plume, ceiling jet, and smoke filling of the adjacent space: Having been driven into the adjacent space by the cross-door pressure differential, the doorway smoke jet is buoyed upward toward the ceiling due to its relatively low density (high temperature). The upward buoyant flow, depicted in Figure 3-10.7, is analogous to the previously discussed fire plume and, with minor modifications, can be quantitatively described by the same kinds of equations. In using these equations, the enthalpy flow rate of the inflowing smoke jet replaces the strength, $\dot{Q}(t)$, of the fire plume, and the smoke jet buoyancy source elevation, taken to be at or near the neutral plane elevation, replaces the elevation of the fire's combustion zone. Further quantitative details on one possible set of door-plume flow calculations are available.²⁵

Just as the doorway smoke jet rises up in the adjacent space, is diluted by entrained fresh ambient air, and is mixed with the upper layer in the manner of a fire plume, so the relatively cool and dense ambient doorway jet enters the fire room, drops down past the upper layer, is contaminated by entrained smoke, and is mixed with the lower layer. This mechanism of lower layer smoke contamination in the room of fire involvement is in addition to the previously described wall flow mechanism which was depicted in Figure 3-10.6.

Figure 3-10.7 depicts the fire environment after the adjacent space upper layer is already well established. At earlier times, adjacent space smoke movement phenomena are closely related to those effects described above (i.e., Figures 3-10.3 and 3-10.4 and associated text) for the room of fire involvement. Thus, the doorway smoke jet plume impinges on the adjacent space ceiling, leads to the development of a ceiling jet which interacts with wall surfaces, and eventually redistributes itself to form a growing, upper layer of uniform thickness.

As was the case for the room of fire involvement, knowledge of adjacent space ceiling and upper wall properties is of fundamental importance in predicting the response of adjacent-space-deployed fire detection/intervention hardware, and the temperature of the adjacent space environment. Also, contamination of the lower layer by smoke injection from downward-directed wall flows can play a relatively more important role in adjacent spaces than in the fire room itself.²³

All the above adjacent room effects must be predicted quantitatively with reasonable accuracy, since the fire-generated environments in the fire room and in adjacent spaces are strongly coupled by cross-door mass and energy exchanges. Also, of key importance is the ability to predict the onset of adjacent space environmental conditions which are untenable for life or property.

Multiroom and multilevel fire/smoke compartments: The discussion in the last two subparagraphs was related to the two-room illustration of Figure 3-10.7. However, the general principles of smoke migration are no different in fire/smoke compartments of more than two connected spaces.

In multiroom or even multilevel compartments, smoke migration occurs as smoke in successive rooms fills to the door/window soffits, and then starts to "spill out" into the adjacent spaces. At the same time, in each room where filling has been initiated, the phenomena related to plumes, ceiling jets, different wall flows, and upper layer/lower layer mixing are also taking place. In each of the spaces, these various phenomena are generally coupled together through the connecting door/window flows. For this reason, all effects must be analyzed simultaneously. For example, in a multiroom fire/smoke compartment one needs to satisfy the principle of conservation of mass when it is applied not just to a single doorway but to all envelopes which completely bound each compartment. To do so, one needs to solve for the pressure difference distributions and the resulting inflows and outflows across all intercompartment penetrations.

Some Special Classes of Multiroom Fire Scenarios

Single room vented to the outside: One practical, special class of the multiroom fire scenario is the single room of fire involvement which is vented to the outside ambient environment. One can carry out an analysis of the fire environment in such vented spaces by bringing to bear all considerations relevant to the Figure 3-10.7 discussion and by assuming the adjacent space to be arbitrarily large, i.e., large enough so that it would never be filled with smoke to the point where such smoke would interact with the fire room itself. The pressure distribution of the adjacent space from the floor to the top of the door/window would be specified to be the same as that of an outside ambient environment.

Dynamics of the plume, which is driven by the smoke flow entering the adjacent space from the fire room, would not be affected by the adjacent space ceiling or far wall surfaces. All inflow to the fire room would be uncontaminated ambient air.

Treating the adjacent space in the above manner leads to considerable simplification in modeling mathematically the room fire environment. It is noteworthy in this regard that the only mathematical models developed specifically to predict post-flashover fire environments are related to this configuration of a single room of fire involvement vented to the outside ambient environment.

Single room vented to large space: Another important class of fire scenario, which is directly related to the last one, is the single room of fire involvement which is actually vented to a very large space. Such is the configuration, for example, when a room of fire involvement is vented to a large atrium.

Under these circumstances one could analyze the fire environment which develops in the large containing space (the atrium) as one would analyze the environment in a space with a single isolated fire (e.g., see Figures 3-10.4 through 3-10.6). Here, the energy and products of combustion release rates of the fire would be taken to be the enthalpy and combustion products' flow rates of the effluent from the doorway/window jet of the fire room. As before (i.e., independent of changes in the large, but finite, adjacent space), and at least for some significant time into the fire, the development of the environment in the fire room itself and the resulting door/window smoke flow could hopefully be predicted analytically. Short of analytic predictions, however, actual measurements of the door/window effluent acquired in full-scale free-burn tests of the fire room, up to and even beyond flashover, could be used as data input in the analysis of the large adjacent space problem.

The combined experimental/analytic approach has been used to predict the environment which develops in large prison cell blocks during fires in single cells of different design.²⁷

Single room and freely connected multiroom fire compartments: For those times of fire development when the compartment of fire involvement consists of a single enclosed space, analysis of the fire environment is considerably simplified. This is because an accounting of inflow and outflow at windows and doors (which are presumably closed) is not required.

When the fire compartment is partitioned into separate but freely connected spaces, the relatively simple, single-enclosed-space analysis, where the area of the single space is taken to be the total area of the fire compartment, can continue to be relevant. Here, "freely connected" refers to fire scenarios and spacial configurations where common openings between rooms are large enough, and/or the energy release rate of the fire is small enough, so that smoke layers remain reasonably uniform in thickness, temperature, and product concentration through the bulk of the compartment area.

Quantitative criteria for establishing whether a specific fire compartment is freely connected relative to a specified fire threat are not yet available. However, the concept of the freely connected, multiroom fire/smoke compartment has been shown to be valid during full-scale multiroom fire experiments.^{2,28}

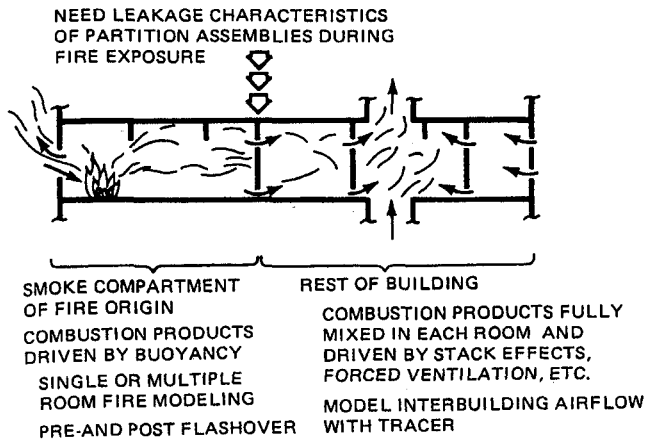


Fig. 3-10.9. A concept for modeling smoke spread throughout complex facilities.

Smoke Spread Outside the Smoke Compartment of Fire Involvement

The above paragraphs addressed the development of the fire-generated environment by describing fire/smoke compartments of fire involvement. Yet, the original outline of the generic firesafety problem is also relevant to the general problem of predicting smoke environments throughout an entire facility.

Figure 3-10.9 illustrates a practical concept for modeling the development of smoke environments both inside and outside the smoke compartment of fire involvement. Facility spaces that would be included in the smoke compartment (on the left of the figure) are distinguished from those included in the rest of the building or facility (on the right) by the detail which is required to describe or model mathematically the fire-generated environments within them. In the smoke compartment of fire involvement, smoke would spread within a room, and would be driven from room to room by strong buoyancy forces which lead to layered smoke environments. These environments must be analyzed in the context of (at least) a two-layer model with associated phenomena of plume flow, surface flows, etc. In the rest of the building, it is reasonable to describe the smoke in each space as being uniformly dispersed. Here, dynamic changes in the smoke distribution in the environment come about from room-to-room pressure differences which are generated by stack effects, wind effects, and forced ventilation, leading to smoke movement, mixing, and dilution.

The fire compartment is the source of smoke to the rest of the building. The rate of introduction of this smoke depends on the pressure differences across common partition assemblies, and on their leakage characteristics.²⁹ Once the rate of smoke leakage across common portions can be expressed quantitatively, the rest of the building problem can be analyzed with a model of smoke movement similar to those presented by Wakamtsu³⁰ and Evers and Waterhouse.³¹

Mathematical Models and Computer Codes for Predicting the Compartment Fire Environment

In recent years, many mathematical models and associated computer codes for predicting dynamic compartment

fire environments have been developed. These can be divided into two types, field models and zone models.

Incorporating global partial differential equations which describe the relevant combustion, flow, and heat transfer processes, field models formulate and solve initial/boundary value problems for the unknown variables in compartment fire scenarios. Zone models, however, describe the compartment fire phenomena in terms of coupled submodel algorithms or sets of equations. Each equation set describes a single fire-generated process associated with an actual physical zone of the compartment space. The processes and corresponding zones typically correspond to the ones identified in Figures 3-10.1 through 3-10.8, and as discussed above.

There is a good deal of variation between all types of compartment fire models. Significant differences tend to be in (1) the number and detail of the individual physical phenomena that are taken into account; (2) the number and complexity of interconnected fire compartment spaces that can be analyzed; and (3) in the most common situation, when a computer is required to solve the model equations, the capability of the computer hardware that is required to carry out the calculations, the user-friendliness of the computer program, and its available documentation.

The intended use for which a given model was developed is probably the most important feature leading to its uniqueness. Such uses can differ widely; for example, at one extreme: to understand and predict coupled, compartment fire-generated processes with the greatest possible accuracy and generality; and at the other: to provide a common-use, firesafety-practitioner's tool for analysis and design. As will be seen, a set of equations which describes the dynamic smoke filling phenomenon in and of itself would constitute a compartment fire model of the simplest variety whose use could fall squarely at the latter extreme of the spectrum.

ASET—A MODEL FOR PREDICTING THE SMOKE FILLING PROCESS IN A ROOM OF FIRE ORIGIN

The smoke filling process is an essential feature of any zone-type compartment fire model. It basically involves three zones: the fire's combustion zone, the plume, and the upper smoke layer. The last section presented a relatively detailed qualitative description of many of the processes which make up the overall dynamic compartment fire environment. This section will formulate a mathematical model of the smoke filling process.

The model to be presented was originally developed within the context of life safety in fires.^{1,2,24} In particular it was developed to provide estimates of the Available Safe Egress Time (ASET) in compartments of fire origin, where the available safe egress time is defined as the length of the time interval between fire detection/successful alarm and the onset of life safety hazard. Accordingly, the model has been given the name ASET.

Since life safety considerations are primary, the model focuses attention on phenomena which develop between the times of fire ignition and the onset of hazardous conditions. This allows significant simplifications in the modeling which would not be otherwise justified, viz., the use of the simplest possible smoke filling process to describe the fire-generated environments of interest.

The basic phenomena of the smoke filling process are outlined as follows:

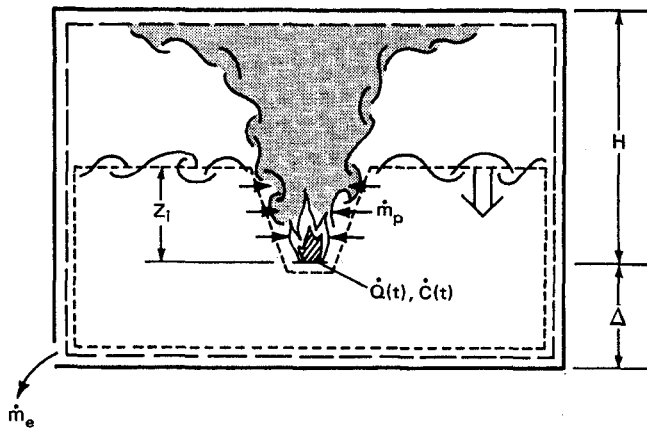


Fig. 3-10.10. Simple illustration of fire-in-enclosure flow dynamics.

The fire starts at some position below the ceiling of the enclosure and releases energy and products of combustion in some time-dependent manner. As the fire develops from ignition, buoyancy forces drive the high-temperature products of combustion upward toward the ceiling. In this way, a plume of upward-moving elevated temperature gases is formed above the fire. All along the axis of the plume relatively quiescent and cool ambient air is laterally entrained and mixed with the plume gases as they continue their ascent to the ceiling. As a result of this entrainment, the total mass flow rate in the plume continuously increases, and the average temperature and average concentration of products of combustion in the plume continuously decrease with increasing height. When the plume gases impinge on the ceiling they spread across it, forming a relatively thin, stably stratified upper layer. As the plume gas upward-filling process continues, the upper gas layer grows in depth, and the relatively sharp interface between it and the cool ambient air layer below continuously drops.

In this section, a simple mathematical model of these phenomena, which captures the essential features of the dynamic fire environment, is constructed. The major elements of the model include the turbulent buoyant plume theory³² together with experimental plume results,³³ the theory of the dynamics of such plumes in confined spaces,³⁴ and the application of the plume dynamics theory to the fire problem as presented.³⁵ Figure 3-10.10 presents a simple illustration of the model's smoke filling flow dynamics. The variables introduced there will be defined in this section.

Initial Value Problem for the Temperature of the Upper Layer and the Position of the Interface

To take a conservative approach, the partitions of the room of fire origin are assumed to have all major penetrations (e.g., doors, windows, and vents) closed. Any leakage from the room resulting from fire-driven gas expansion is assumed to occur near the floor level. The sketch of Figure 3-10.7 is compatible with these assumptions, both of which lead to some conservatism in the eventual prediction of the time for onset of untenability.

The fire's combustion zone is modeled as a point source of energy release which is effectively located at or above the floor level. The mass flow rate of fuel introduced from this

zone into the plume is neglected compared with the mass flow rate of entrained air. Except for the buoyancy forces that they produce, density variations in the flow field are neglected (i.e., the Boussinesq approximation is invoked). Using the fact that the absolute pressure throughout the space varies only insignificantly from a constant uniform value, the density, ρ , can be related to the absolute temperature, T , at any time and spatial position through the perfect gas law according to

$$\rho T = \text{Constant} = \rho_a T_a \quad (1)$$

where ρ_a and T_a are the density and absolute temperature, respectively, of the ambient air.

The time-varying total energy release rate of the combustion zone is defined by $\dot{Q}(t)$. It is assumed that $\dot{Q}(t)$ can be approximated by the free-burn energy release rate of the characteristic fuel assembly whose hazard-producing characteristics are under investigation and for which $\dot{Q}(t)$ is known. This assumption is consistent with the fact that onset of hazardous conditions within the enclosure will occur at temperature and depleted-oxygen levels which are low compared with those levels at which variations from free-burn will begin to be significant.

The fraction of \dot{Q} which effectively acts to heat the plume gases and to ultimately drive the plume's upward momentum is $(1 - \lambda_r)$, where λ_r is approximately the fraction of \dot{Q} lost by radiation from the combustion zone and plume.

The total mass flow in the plume, \dot{m}_p , and the mass mixing cup temperature of the plume, \bar{T}_p , at a distance Z above the fire (but below the layer interface) can be estimated by^{7,35}

$$\bar{T}_p/T_a - 1 = (\dot{Q}^*)^{2/3}/0.210, \quad 0 < Z \leq Z_i(t) \quad (2)$$

$$\dot{m}_p = 0.210\rho_a(gZ)^{1/2}Z^2(\dot{Q}^*)^{1/3}, \quad 0 < Z \leq Z_i(t) \quad (3)$$

where \dot{Q}^* is defined as

$$\dot{Q}^* = (1 - \lambda_r)\dot{Q}/[\rho_a C_p T_a (gZ)^{1/2}Z^2]$$

and where g is the acceleration of gravity, C_p is the specific heat at constant pressure, assumed to be constant and uniform throughout the space, and $Z_i(t)$ is the time-varying distance above the fire of the interface which separates a growing upper layer of elevated-temperature (product of combustion-laden gas) and a lower shrinking layer of ambient air. The mass flow rate of gas, \dot{m}_e , leaking out of the room's floor-level leakage paths can be estimated from³⁵

$$\dot{m}_e = \begin{cases} (1 - \lambda_c)\dot{Q}/(C_p T_a), & -\Delta < Z_i(t) \\ (1 - \lambda_c)\dot{Q}/(C_p \bar{T}_h), & -\Delta = Z_i(t) \end{cases} \quad (4)$$

where Δ is the height of the fire above the floor, and λ_c is the instantaneous fraction of \dot{Q} lost to the bounding surfaces of the room and its contents (i.e., $\lambda_c = \dot{Q}_{loss}/\dot{Q}$). Also, assuming that the upper layer is well mixed, \bar{T}_h is taken to be its absolute temperature. By using Equation 2, \bar{T}_h can be related to the average upper layer density, $\bar{\rho}_h$, which is defined by

$$\bar{\rho}_h = \frac{1}{(H - Z_i)} \int_{Z_i}^H \rho dZ \quad (5)$$

The total rate of energy loss characterized by λ_c occurs as a result of a variety of convective and radiative heat transfer exchanges between the room's gases and the above-mentioned

surfaces. Equation 6 brings attention to the fact that, by the time the layer interface drops to the floor, i.e., when $Z_i = -\Delta$, all ambient air has been pushed out of the room. At all subsequent times, the entire room is filled with, and defines the bounds of, the upper layer, and the room's leakage gases are at upper layer rather than ambient conditions.

A mass balance for the lower, shrinking volume of ambient air results in

$$\rho_a A \frac{dZ_i}{dt} = \begin{cases} -\dot{m}_e - \dot{m}_p(Z = Z_i), & 0 < Z_i(t) \leq H \\ -\dot{m}_e, & -\Delta < Z_i(t) \leq 0 \\ 0, & -\Delta = Z_i(t) \end{cases} \quad (6)$$

where A is the area and H is the height of room of fire origin, and where estimates for \dot{m}_e and \dot{m}_p are provided in Equations 3 and 4.

Using Equations 2 and 7 in an energy balance for the upper layer results in

$$1 - \bar{\rho}_h/\rho_a = 1 - T_a/\bar{T}_h \\ = \left[\int_0^t (1 - \lambda_c) \dot{Q} d\xi \right] / [\rho_a C_p T_a A (H - Z_i)], \quad (7) \\ -\Delta < Z_i < H$$

$$(1 - \lambda_c) \dot{Q} = (\Delta + H) \rho_a C_p T_a A (1/\bar{T}_h) d\bar{T}_h/dt, \quad Z_i = -\Delta \quad (8)$$

Equations 4 and 6 are now used in Equation 6, and Equation 7 is recast into differential form. After some manipulation, the following pair of governing equations for Z_i and \bar{T}_h result

$$\frac{dZ_i}{dt} = \begin{cases} -C_1 \dot{Q} - C_2 \dot{Q}^{1/3} Z_i^{5/3}, & 0 < Z_i \leq H \\ -C_1 \dot{Q}, & -\Delta < Z_i \leq 0 \\ 0, & Z_i = -\Delta \end{cases} \quad (9)$$

$$\frac{d\bar{T}_h}{dt} = \begin{cases} \bar{T}_h [C_1 \dot{Q} - (\bar{T}_h/T_a - 1) C_2 \dot{Q}^{1/3} Z_i^{5/3}] / (H - Z_i), & 0 < Z_i \leq H \\ \bar{T}_h C_1 \dot{Q} / (H - Z_i), & -\Delta \leq Z_i \leq 0 \end{cases} \quad (10)$$

$$\left. \begin{aligned} C_1 &= (1 - \lambda_c) / (\rho_a C_p T_a A) \\ C_2 &= (0.21/A) [(1 - \lambda_r) g / (\rho_a C_p T_a)]^{1/3} \end{aligned} \right\} \quad (11)$$

The problem now becomes one of simultaneously solving Equations 9 and 10 subject to the appropriate initial conditions. For the present purpose, these initial conditions can be taken as those relating to one of two different cases.

Case 1: $\dot{Q}(t=0) \equiv \dot{Q}_0 \neq 0$.
Here assume

$$\lim_{t \rightarrow 0} \dot{Q} \approx \dot{Q}_0 + \dot{Q}'_0 t \quad (12)$$

where

$$\dot{Q}'_0 = \frac{d\dot{Q}}{dt} \quad \text{at } t = 0$$

Then, solve Equations 9 and 10 subject to the initial conditions

$$\begin{aligned} Z_i(t=0) &= H \\ \bar{T}_h(t=0) &= T_a [1 + (C_1 \dot{Q}_0^{2/3}) / (C_2 H^{5/3})] \\ &= T_a + [(1 - \lambda_c) / (1 - \lambda_r)] [\bar{T}_p(t=0) - T_a] \end{aligned} \quad (13)$$

where the value for $\bar{T}_h(t=0)$ was obtained with the use of Equation 7. Using Equation 7 further, an analysis of the apparent singularity of Equation 10 at $t=0$ leads to the result

$$\lim_{t \rightarrow 0} \frac{d\bar{T}_h}{dt} = T_a (C_1/C_2) [\dot{Q}_0^{2/3} / (6H^{8/3})] \cdot [2\dot{Q}'_0 H / \dot{Q}_0 + 5(C_1 \dot{Q}_0 + C_2 H^{2/3} \dot{Q}_0^{1/3})] \quad (14)$$

Case 2: $\dot{Q}(t=0) = 0$
Here assume

$$\lim_{t \rightarrow 0} \dot{Q} \approx \dot{Q}'_0 t \quad (15)$$

Then solve Equations 9 and 10 subject to the initial conditions

$$Z_i(t=0) = H, \quad \bar{T}_h(t=0) = T_a \quad (16)$$

In this case, analysis of the problem leads to the following small time estimates

$$\lim_{t \rightarrow 0} Z_i \approx H - (3/4) C_2 \dot{Q}'_0^{1/3} H^{5/3} t^{4/3} \quad (17)$$

$$\lim_{t \rightarrow 0} \bar{T}_h \approx T_a + (2/3) T_a (\dot{Q}'_0)^{2/3} / H^{5/3} (C_1/C_2) t^{2/3} \quad (18)$$

Safe Available Egress Time from the Solution to the Initial Value Problem for Upper Layer Thickness and Temperature

The above initial value problem for Z_i and \bar{T}_h would be solved by a numerical integration procedure. For the purpose of using the equations to determine onset of hazardous conditions, the solution would be terminated in a given problem at the time, t_{HAZ} , when

$$\bar{T}_h \geq \bar{T}_{h(HAZ)} \quad (19)$$

(layer temperature reaches a hazardous value associated with an untenable flux of thermal radiation)

or

$$Z_i \leq Z_{i(HAZ)} \quad (20)$$

(interface reaches a characteristic face elevation, $Z_{i(HAZ)}$, and the upper layer gases are assumed to be hazardous for human ingestion or significantly impairing to human vision).

From the computed history of Z_i and \bar{T}_h , and compatible with the detection criterion which is invoked, the time of detection could also be obtained. This would be defined as that time, t_{DET} , when, for example,

$$\bar{T}_h \geq \bar{T}_{h(DET)} \quad (21)$$

(layer temperature detection criterion)

and/or

$$d\bar{T}_h/dt \geq (d\bar{T}_h/dt)_{DET} \quad (22)$$

(layer rate of temperature rise detection criterion).

The time of detection corresponding to other detection criteria which were similarly related to Z_i and \bar{T}_h , etc., could also be obtained. Finally, the time of detection could be explicitly specified, e.g., "immediate" detection, $t_{DET} = 0$, as a result of the guaranteed presence of alert occupants.

From all the above, the desired value for ASET is computed from

$$ASET = t_{HAZ} - t_{DET}$$

The computer program ASET has been developed to carry out the solution to the above problem for arbitrarily specified $\dot{Q}(t)$. The program is written in American National Standards Institute (ANSI) FORTRAN and it is supported by a user's manual.²⁴

A simplified version of the program, ASET-B, written in BASIC and containing all necessary equation-solving software, has also been developed, and it is supported by its own user's manual.³⁶

Initial Value Problem for the Concentration of Products of Combustion

In this subsection, equations for estimating the concentration of products of combustion in the upper layer are developed.

The time-varying rate at which a combustion product of interest is generated within the combustion zone is designated by $C(t)$. The dimensions of $C(t)$ are u_c per unit time, where u_c is a dimensional unit appropriate for the particular product. For example, u_c could have the dimensions of mass, number of particles, number of particles with mass between m and $(m + dm)$, etc.

Just as $\dot{Q}(t)$ is approximated by free-burn energy release rate data, so it is assumed that $C(t)$ can be approximated by the free-burn product generation rate of the fuel assembly under investigation. As is the case with \dot{Q} , C is assumed to be known, say, from experimental free-burn measurements.

The average concentration of product in the upper layer is defined as the average amount of product (dimension u_c) per unit mass of upper layer mixture. The concentration is designated by $M(t)$. It is assumed that the mass fraction of the product in the upper layer is always small compared to 1.

Conservation of the product results in

$$\frac{d}{dt}[\bar{\rho}_h MA(H - Z_i)] = \dot{C}, \quad -\Delta < Z_i \leq H \quad (23)$$

$$\frac{d}{dt}[\bar{\rho}_h MA(H + \Delta)] = \dot{C} - \dot{m}_e M, \quad Z_i = -\Delta \quad (24)$$

Manipulation of Equations 23 and 24 with the use of Equations 9 and 10 leads to the following equation for M

$$\frac{dM}{dt} = \begin{cases} [\bar{T}_h/(T_a \rho_a A)] \\ \{\dot{C} - \rho_a AC_2 \dot{Q}^{1/3} Z^{5/3} M\}/(H - Z_i), & 0 < Z_i < H \\ [\bar{T}_h/(T_a \rho_a A)] \dot{C}/(H - Z_i), & -\Delta \leq Z_i \leq 0 \end{cases} \quad (25)$$

With solutions for Z_i and \bar{T}_h from earlier considerations, Equation 25 can be solved for M once appropriate initial conditions are established. For this purpose, the two cases must be considered again.

Case 1(a): $\dot{Q}(t = 0) \equiv \dot{Q}_0 \neq 0$; $\dot{C}(t = 0) \equiv \dot{C}_0 \neq 0$.
Here assume

$$\lim_{t \rightarrow 0} \dot{C} \approx \dot{C}_0 + \dot{C}'_0 t \quad (26)$$

where

$$\dot{C}'_0 = \frac{d\dot{C}}{dt} \quad \text{at } t = 0$$

Then, solve Equation 25 subject to

$$M(t = 0) = \dot{C}_0/(C_2 A H^{5/3} \rho_a \dot{Q}_0^{1/3}) = \dot{C}_0/\dot{m}_p(t = 0) \quad (27)$$

Here, an analysis of the apparent zero time singularity of Equation 25 leads to the result that

$$\lim_{t \rightarrow 0} \frac{dM}{dt} = \left(\frac{5}{6}\right)(C_1/C_2)[\dot{Q}_0^{2/3} \dot{C}_0/(\rho_a A H^{8/3})] \cdot [1 + H(3\dot{C}'_0/\dot{C} - \dot{Q}'_0/\dot{Q}_0)/(5\dot{Q}_0 \dot{C}_1) + (C_2/C_1)(H^{5/3}/\dot{Q}_0^{2/3})] \quad (28)$$

Case 1(b): $\dot{Q}(t = 0) \equiv \dot{Q}_0 \neq 0$; $C(t = 0) \equiv C_0 \neq 0$.
Here assume

$$\lim_{t \rightarrow 0} \dot{C} \approx \dot{C}_0 t \quad (29)$$

Then, solve Equation 25 subject to

$$M(t = 0) = 0 \quad (30)$$

In this case, analysis of Equation 25 leads to the following small time estimate

$$\lim_{t \rightarrow 0} M = \dot{C}'_0 t / (2\rho_a A^{5/3} Q^{1/3} C_2) = \dot{C}'_0 t / [2\dot{m}_p(t = 0)] \quad (31)$$

Case 2(b): $\dot{Q}(t = 0) = 0$; $\dot{C}(t = 0) = 0$.
(Note that the condition $\dot{Q}(t = 0) = 0$, $C(t = 0) \neq 0$, i.e., nonzero product generation rate with a zero heat release rate, is not allowed.) Here assume Equation 29. Then solve Equation 25 subject to Equation 30. In this case, analysis of Equation 25 leads to

$$\lim_{t \rightarrow 0} M = 2\dot{C}'_0 t^{2/3} / (3\rho_a AC_2 H^{5/2} \dot{Q}_0^{1/3}) \quad (32)$$

Using Combustion Product Concentrations to Establish the Time of Detection and the Onset of Untenability

When a fire's rate of generation of products of combustion is known, the upper layer concentrations can be estimated from the considerations of the previous section. Under such circumstances, it would be possible to apply detection and hazard criteria which are more detailed than those discussed earlier.

In the case of detection, the response of a detection device which is sensitive to the presence of the predictable combustion product can be simulated. For example, the time of detection, t_{DET} , would be predicted to be the time when the upper layer concentration of the product attained a detectable level, M_{DET} .

In the case of hazard, a criterion for the onset of untenability could depend on a variety of possible conditions involving all of the environmental parameters, Z_i , \bar{T}_h , and M . For example, assume that estimates of the fire's generation rate of water and CO are available. Then, the time-varying values for Z_i , \bar{T}_h , M_{water} , and M_{CO} could be computed, and the time of onset of untenability could be estimated to be the earliest time when (1) the interface was still above a

characteristic elevation, Z_F , and \bar{T}_h exceeded a specified hazardous overhead value (associated with an untenable flux of thermal radiation), or (2) the interface was below Z_F , and the upper layer CO concentration or temperature and humidity conditions were such as to be hazardous for human ingestion.

All of the above considerations are taken into account in the ASET computer program. Predictions of product of combustion concentration are not yet included in ASET-B.

AVAILABLE SAFE EGRESS TIME FROM ROOMS OF FIRE ORIGIN— SOME EXAMPLE CALCULATIONS

Assumptions on the Disposition of Energy Release and Their Implications

In order to use the proposed fire model for a specified free-burn fire, values of λ_r and λ_c are required. While appropriately chosen constant- λ values should prove to be adequate for most engineering applications, the model described can, through specified dynamic variations in these λ s, readily accept more detailed characterizations of the gas-to-room surface heat transfer phenomena.

Depending on the fuel and its configuration, the total radiant power output in fire combustion zones is in the range of 15 to 40 percent of the total rate of heat release.^{38,39} Based on this and, for example, on data presented by Cooper,⁴⁰ it appears that $\lambda_r = 0.35$ is a reasonable choice for the type of growing hazardous fires under consideration. Except where noted otherwise, this value will be used in all calculations described in this chapter.

Using the 0.35 value for λ_r , and taking account of convective heat transfer considerations, an appropriate value for λ_c was developed.⁴¹ It was found to lie in the approximate range 0.6 to 0.9. The lower value, 0.6, would relate to high aspect ratio spaces (ratio of ceiling span to room height) with smooth ceilings and with fires positioned far away from walls. The intermediate values and the high, 0.9, value for λ_c would relate to low aspect ratio spaces, fire scenarios where the fire position is within a room height or so from walls and/or spaces with highly irregular ceiling surfaces. In the latter types of situations, which are representative of most realistic fire scenarios, it is not presently possible to provide general rules to accurately estimate λ_c within this 0.6 to 0.9 range. This fact has strong implications on the capability for establishing accurate estimates for the average upper layer temperature. This can be seen from Equation 10, where, early in the fire and at times of relatively cool upper layer temperatures (\bar{T}_h/T_a close to 1), $d\bar{T}_h/dt$ and, ultimately, $\bar{T}_h - T_a = \Delta\bar{T}_h$ are seen to be proportional (through the factor C_1) to $(1 - \lambda_c)$. In contrast to the upper layer temperature estimate and at times of relatively small values of $\Delta\bar{T}_h/T_a = \bar{T}_h/(T_a - 1)$, the upper layer-lower layer interface position history is not nearly as sensitive to inaccuracies in λ_c . At such times, the second term on the right-hand side of the first line of Equation 9, which is independent of λ_c , will dominate the first term, the two terms being in the ratio of \dot{m}_p to \dot{m}_e (compare to the first line of Equation 6).

The above discussion leads to the following guidelines for selection and use of a value for λ_c , when a reliable estimate of its actual value is not otherwise available:

1. For the purpose of computing a conservative estimate of the time when a hazardous temperature or a hazardous

interface elevation will be attained (i.e., the predicted t_{HAZ} will be less than the observed t_{HAZ}), one should select $\lambda_c = 0.6$.

2. For the purpose of a conservative estimate of detection time when detection is by temperature or rate of temperature rise of the upper layer (i.e., the predicted t_{DET} will be greater than the actual t_{DET}), one should select $\lambda_c = 0.9$.
3. When fire detection is by temperature or rate of temperature rise, a reasonably accurate (as compared with a conservative) estimate of detection time is achievable only (1) in large aspect ratio, smooth ceiling spaces where detection is based on a $\lambda_c = 0.6$ computation of average upper layer temperature, and (2) in other configurations where detectors are deployed near the ceiling in some regular grid array, and where the time of detection is based on estimates of actual maximum ceiling-jet temperature (i.e., predictions of average upper layer temperature are not the basis for determining likely time of detection). For such estimates, the reader is referred to Section 4, Chapter 1 of this handbook.

Available Safe Egress Time in a Semi-Universal Fire

For the smoke filling model to have utility to practitioners of fire safety, it is necessary that the significant elements of potentially threatening fire scenarios be identified. It is also necessary for the results of fire hazard analyses to be presented in a concise and practical manner. This subsection provides an example of how the whole concept might proceed in practice.

First, one must identify quantitative characteristics of a particular, potentially threatening, free-burn fire of concern. Cooper deals with some practical considerations that would be useful in deducing such characteristics.¹ For the present, a composite, semi-universal-type fire has been constructed from the data of Friedman.⁴¹ The fire's energy release history is plotted in Figure 3-10.11. The fire is assumed to be initiated from a 10 kW ignition source. Initially, it grows exponentially at a rate which is characteristic of a fire initiated in a polyurethane mattress with bedding. This early growth rate would be characteristic of the early growth of fires in a variety of occupancies which typically contain upholstered polyurethane cushioning, e.g., hospital patient and lobby rooms, residential spaces, and auditoriums. It is also consistent with the (unreported) early growth state of fires in large assemblies of commodities stacked on pallets. Beyond 400 kW, the fire of Figure 3-10.11 is assumed to grow at a rate which is similar to and/or which bounds the anticipated growth of fires initiated in a variety of different types of commodities stacked on pallets. The portion of the semi-universal fire beyond 400 kW is no doubt also representative of other threatening fires in large mercantile and/or business occupancies.

The fire of Figure 3-10.11 was assumed to be initiated in a variety of different-size spaces. The geometries of these spaces are characterized by areas ranging from 28 to 929 m² and by heights ranging from 2.4 to 6.1 m.

Two possible criteria for fire detection are considered in the analysis of available safe egress time. These include using ASET to calculate instantaneous detection (by whatever means) and detection when the upper gas layer reaches an average temperature of 57°C. The utility of the latter detection criterion is at present strictly speculative. It is included here only to illustrate the type of results which one

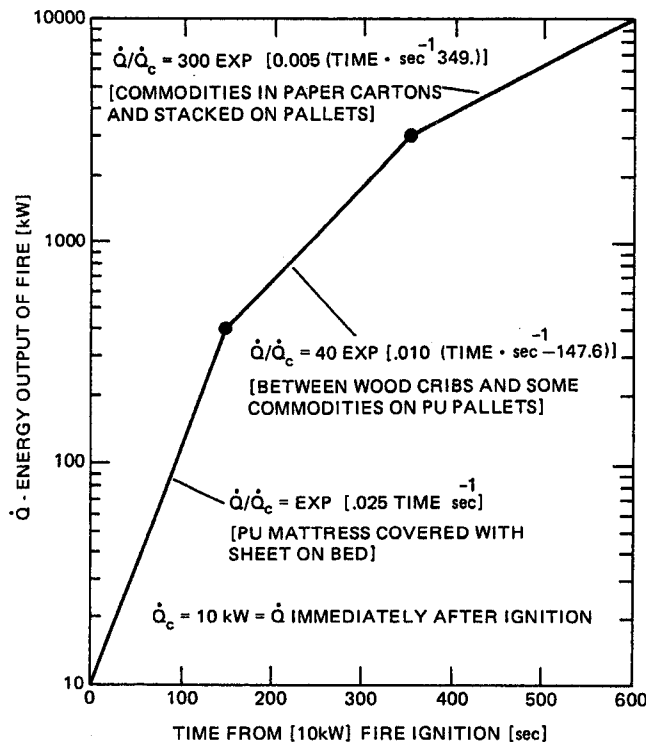


Fig. 3-10.11. Free-burn energy release rate from a semi-universal fire. A fictitious construction from the data of O'Neill and Hayes.⁴⁴

might hope to generate by solution of the model equations and use of the ASET computer program. (The results could also be obtained with ASET-B.)

The criterion adopted for the onset of hazardous conditions is an upper layer interface position 0.91 m above the floor, or an average upper layer temperature of 183°C (corresponding to a heat flux of 0.25 W cm⁻² at the floor), whichever comes first.

It is assumed that 35 percent of the fire's instantaneous energy release rate is radiated from the combustion zone ($\lambda_r = 0.35$) and that a total of 60 percent of this energy release rate is transferred to the interior surfaces of the room and its contents, i.e., 40 percent of this energy is retained in the upper layer products of combustion ($\lambda_c = 0.60$). Recall that the latter choice of λ_c would be appropriate for large aspect ratio spaces with smooth ceiling, but, in any event, the choice of λ_c would have a minor impact on estimated egress times in cases where criteria of detection or hazard are not dependent on upper layer gas temperature.

With the above range of parameters, the quantitative details of the last section were used to estimate available safe egress times with the ASET program. The results of these computations are presented in Figure 3-10.12. In this figure, $ASET = t_{HAZ} - t_{DET}$ is plotted as a function of room area for different parametric values of room height and for different detection criteria.

As an example of the utility of Figure 3-10.12, consider a scenario where a fire is initiated in an occupied, 500 m², nominal, 6.1 m-high auditorium outfitted with polyurethane cushion seats (which are assumed to be the most significant fuel load). Then, from Figure 3-10.12 one would estimate an available safe egress time of approximately 450 s.

This assumes immediate detection as a result of occupant recognition and verbal alarm to fellow occupants at the time of fire initiation. If the auditorium is to be considered safe relative to successful egress, then a further study would have to reveal that the time required for a capacity crowd to evacuate the auditorium is less than 450 s.

The following general features of the results of Figure 3-10.12 are worth noting:

1. As is well known, for life safety as it relates to safe egress, temperature detectors are not particularly effective.
2. For a given curve, increasing room area eventually leads to an abrupt reduction in the curve's slope. This is the result of a shift in the triggering mechanism for onset of hazardous conditions. On the left side of the change in slope (smaller areas), untenability occurs as a result of the layer interface dropping to the 0.91 m level. On the right side (larger areas), untenability occurs as a result of thermal radiation from a hot upper layer.

Based on the previously developed model equations, the calculation procedure described in this section has been generalized and incorporated with other example calculations into the ASET computer program user's manual.²⁴ For a fire scenario of interest, this computer program carries out ASET calculations corresponding to user-supplied inputs which describe the fire threat, room size, and appropriate user-specified detection and hazard criteria.

A POSSIBLE EXTENSION IN THE MODEL'S UTILITY

An Experimental, Full-Scale, Multi-Room Fire Scenario

This section compares the results of a full-scale, multi-room fire experiment with calculations based on ASET. The experiment was one of a series of tests in a mockup hospital patient room/corridor building space.⁴⁴

A plan view of the building space is presented in Figure 3-10.13. The space is made up of a room of area 14.4 m² connected by an open doorway to a corridor-lobby configuration of area 74.3 m².

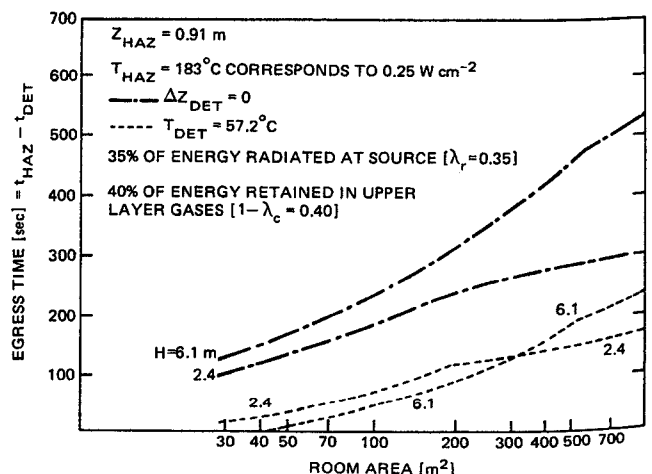


Fig. 3-10.12. Estimates of available egress times from the semi-universal fire of Figure 3-10.11.

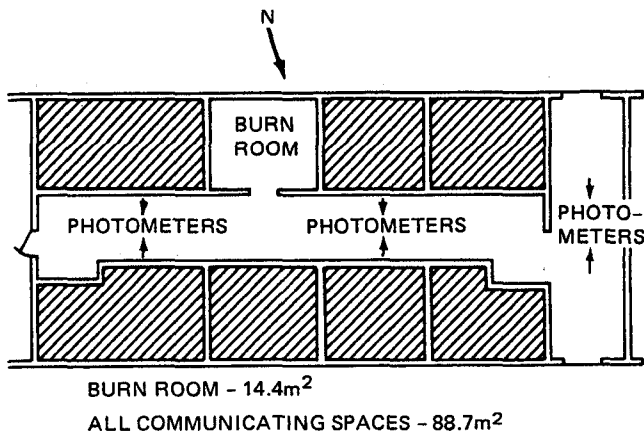


Fig. 3-10.13. Plan view of hospital room/corridor mockup space.

A fire is initiated in a wastepaper basket next to the corner of a polyurethane mattress covered with bedding. The burn characteristics of this assembly were studied prior to the room burns of this series.⁵ The wastepaper basket/mattress fuel energy release rate, as derived from weight loss measurements, is plotted in Figure 3-10.14. For the purpose of the present analysis, it is assumed that this energy release rate was reproduced in the actual test run under review.

The model, which has been quantitatively described so far, is a single-room or room-of-fire-origin model. Thus, it may not be immediately obvious at what point, if any, it will have relevance to the present fire scenario. It would appear that a two-room or multi-room flow dynamics model would generally be required to study the room-corridor-lobby scenario under consideration. (For example, a two-room example flow calculation for a set of fire and room size parameters which somewhat corresponds to the present scenario has been considered.)²⁵ Nevertheless, it is possible that a simple, single-room modeling approach to fire scenarios involving relatively free-flowing multi-space configurations can be adequate for the purpose of obtaining engineering estimates of available egress times in the range of conditions that occurred in the referenced hospital patient room/corridor test.

Model Predictions Compared with Experimental Results

Room of fire origin: For early times into the fire, prior to the time when the upper layer interface drops to the level of the connecting doorway soffit, the single-room model is completely relevant. Up to that moment, the open doorway acts as the lower leakage path referred to earlier. Using the energy release data of Figure 3-10.14, and taking the fire source to be effectively at the floor, the model was used to compute the product of combustion-filling history of a 14.4 m² room up to the time that the upper layer thickness exceeded the existing ceiling-to-soffit dimension of 0.41 m. λ_c was estimated at 0.72.⁴⁰ The time for the interface to reach the soffit was computed to be 21 s, following ignition.

Adjacent space: Once the smoke flows under the soffit and starts to fill the large corridor-lobby space, a two-room model is required to describe the gas migration and exchange between the two spaces. This would continue to be true for at least some intermediate time interval. Following this, the single-room model can again be relevant.

If the fire is small enough or the doorway is large enough so that flows through the doorway remain relatively weak, the adjacent space will eventually attain and maintain a smoke layer thickness essentially identical to that of the room of fire origin. After some time interval, the histories of the elevations of the layer interfaces in both the corridor/lobby and room of fire origin spaces will be similar and can be computed from a single-room model, where the single room has an area equal to the combined area of both spaces. Time intervals when the upper layer thickness of the two rooms is not similar would encompass (1) the initial time when the room of fire origin fills up with smoke to the level of the doorway soffit, and (2) the subsequent time interval when the upper layer thickness of the adjacent space grows from zero to a value close to that of the room of fire origin.

For fire scenarios where the above is applicable, significant simplifications occur in that the relatively simple single room of fire origin model can be used to study the effects of fire growth when far more complicated multi-room models would, at first hand, appear to be required.

To test the above ideas, the single-room model was used to predict the history of a single interface elevation and the average upper layer temperature within the combined patient room/corridor space. Using the energy release rate of Figure 3-10.14 and a total room area of 88.7 m², the history of the interface elevation and of the average upper layer temperature was computed. An effective λ_c for this combined space scenario is expected to be greater than the above $\lambda_c = 0.72$ value used for the single room of fire origin because of the additional heat transfer to the corridor surfaces. A value of $\lambda_c = 0.85$ was selected for the calculation. This was done with the anticipation that comparisons between computed and experimental average upper layer temperatures would reveal an appropriate correction to this λ_c value. (Recall that the upper layer temperature difference, $\Delta \bar{T}_h$, is

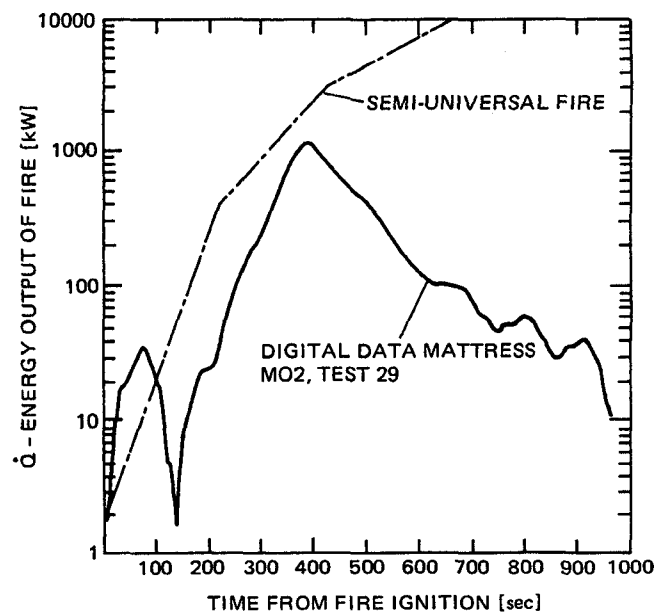


Fig. 3-10.14. Energy release rate of wastepaper basket/mattress fuel assembly.

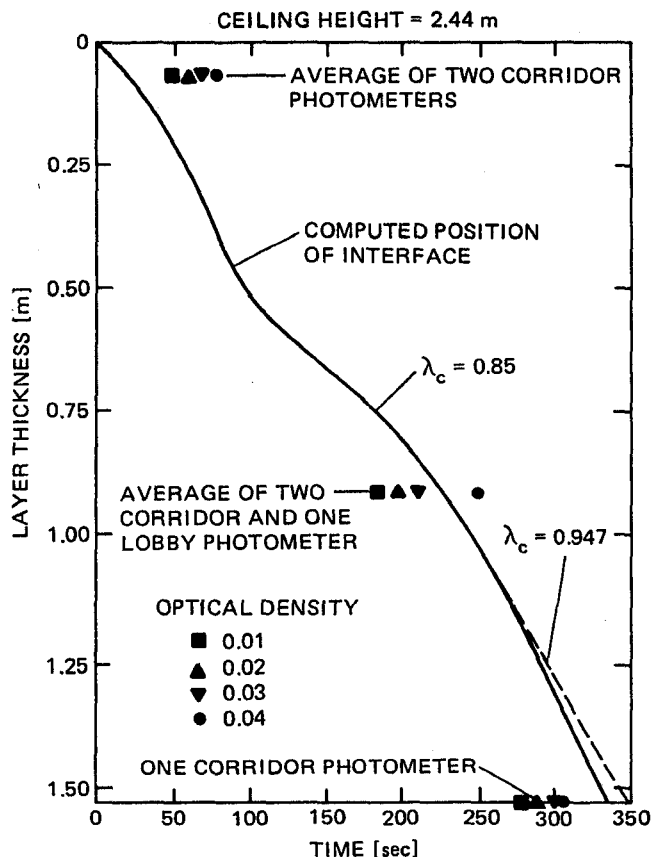


Fig. 3-10.15. History of interface position.

approximately proportional to $1 - \lambda_c$.) The results of the computation for interface position and upper layer temperature are presented in Figures 3-10.15 and 3-10.16, respectively.

For the purpose of comparing results for the analytic and experimental interface position, an operational definition of the experimental interface position was required. This definition was based on the outputs of a total of six photometers placed at three different elevations and at one to three different positions (see Figure 3-10.13) in the corridor and lobby. The measured optical density (OD) outputs of these photometers are indicated in Figure 3-10.17. From these outputs, and for the purpose of defining a time when the smoke layer interface position passes the elevations of these photometers, there is still ambiguity as to what value of OD should constitute the presence of a smoke layer. Four different OD values, 0.01, 0.02, 0.03, and 0.04, were used as possible definitions for a minimum upper layer OD. Using the photometer outputs, the result of these four possible interface definitions leads to four possible sets of experimental data points for the interface elevation versus time. These are plotted in Figure 3-10.15 together with the theoretical results of the interface motion.

The favorable agreement between the results of theoretical and experimental interface position at the lower two of the three photometer locations illustrates the capability of the single-room model, in the present multi-room fire scenario, to predict the growth of the potentially hazardous upper smoke layer thickness. A favorable comparison at the uppermost photometer elevation located 0.06 m from the

ceiling was not to be expected. This is because of the fact that, in the present multi-space configuration, the single-room model implemented in the manner described is clearly not adequate to predict the early growth in the corridor-lobby portion of the test space. Subsequent testing in the Figure 3-10.13 test space has corroborated the potential utility of the model in providing practical simulations of multi-room fire environments.²⁸

Gas temperatures were measured by two thermocouple trees located in the center of the corridor 4.6 m on either side of the room of fire origin doorway. No temperature data were acquired in the lobby space. At any given time, the elevation thermocouples of these two trees measured temperature differences, $(T - T_a)$, which agreed to within 20 percent of one another. For the purpose of comparing analytic and experimental average upper layer temperature histories, an appropriate instantaneous weighting of the measured temperatures of the limited number of these corridor thermocouples was required. At a given instant of time, this weighing has to be consistent with the estimate/measurement of the interface position as well as with the relative position of the thermocouples in question. A plot of the measured average upper layer temperature history deduced from such a data reduction scheme is presented along with the plot of the computed temperature history in Figure 3-10.16. As noted earlier, if a different λ_c has been used in the computation then, to a first approximation (i.e., using the principle of proportionality between $\Delta\bar{T}_h$ and $1 - \lambda_c$), one would anticipate a shift from the originally computed $\Delta\bar{T}_h(t)$ (with $\lambda_c = 0.85$) to a new temperature history $\Delta\bar{T}_h^{(new)}(t)$ [with $\lambda_c = \lambda_c^{(new)}$], where

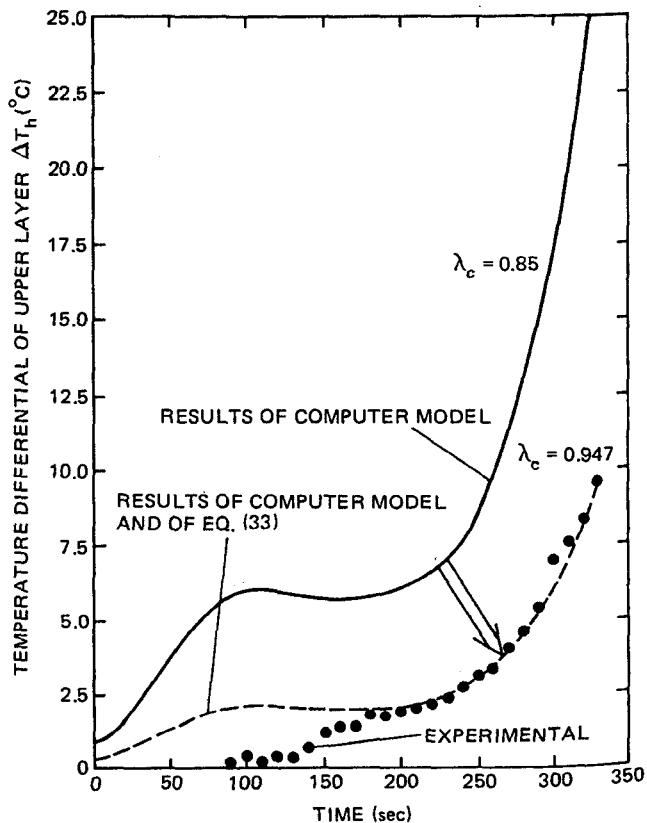


Fig. 3-10.16. History of average upper layer temperature.

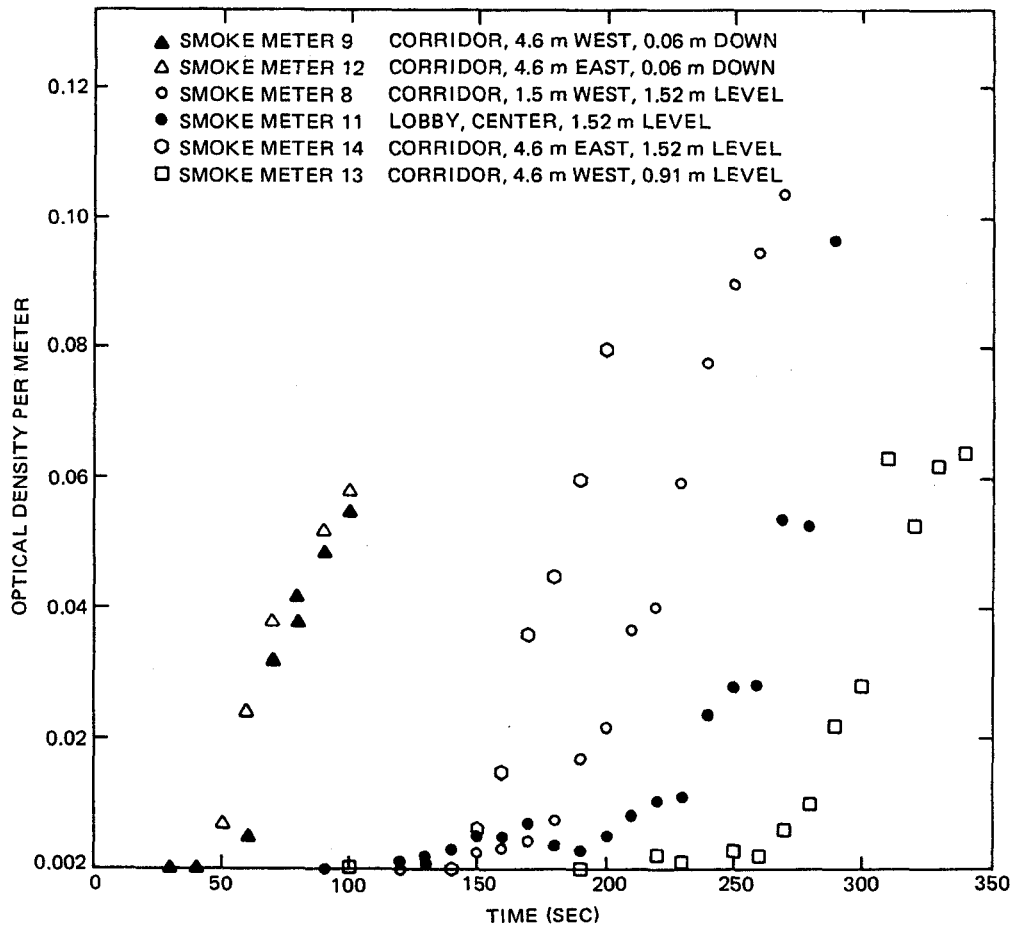


Fig. 3-10.17. Optical densities measured by the photometers.

$$\Delta \bar{T}_h^{(new)}(t) = [(1 - \lambda_c^{(new)}) / (1 - 0.85)] \Delta \bar{T}_h(t) \quad (33)$$

In view of the above, it is possible to bring the predicted analytic \bar{T}_h plot into coincidence with the experimental \bar{T}_h plot for at least one instant of time by a new choice, $\lambda_c^{(new)}$, for λ_c . Such coincidence is attained at $t = 330$ s (when the computed layer interface is at the potentially hazardous position 0.91 m from the corridor floor) by the specific choice of $\lambda_c^{(new)} = 0.947$. Using this latter value of $\lambda_c^{(new)}$ in Equation 33, an adjusted average upper layer temperature history was computed and plotted. (See Figure 3-10.16.)

The single-room model was also used to recompute the interface position and temperature histories corresponding to $\lambda_c = 0.947$. These are plotted in Figures 3-10.15 and 3-10.16, respectively. For the parameters of the present scenario, the proximity of the $\lambda_c = 0.85$ and $\lambda_c = 0.947$ plots of Figure 3-10.15 illustrates the relative insensitivity of the interface position history to changes in λ_c . The variations between the two $\lambda_c = 0.947$ temperature history estimates are so small that they cannot be discerned in most of the Figure 3-10.15 plot. For this scenario, this illustrates the insensitivity of interface position on λ_c .

As can be noted in Figure 3-10.16, the experimental and newly calculated estimates for the upper layer temperature history are in good agreement in the time interval 175–330 s but in poor agreement at earlier times. Besides the fact that

earlier times are likely to require analysis by a multi-room model, it is worth noting that the relatively complicated nature of the energy transfers which are being simulated may preclude sharper estimates of \bar{T}_h with a single, constant value of λ_c . In this regard, results indicate that for fires in the present test space, λ_c can vary in time over a wide range of values.²⁸

SOLUTIONS TO THE MODEL EQUATIONS FOR A SPECIAL CLASS OF GROWING FIRES

As was indicated in the last two sections, the ASET smoke filling model equations are easily solved with the use of the ASET or ASET-B computer programs for any particular fire specified by $\dot{Q}(t)$, $\dot{C}(t)$, and parameters H , A , Δ , λ_r , and λ_c . However, the approach of solving the equations for one set of conditions at a time does not lead readily to insight into solutions of generic problems of interest. For example, to obtain the results of Figure 3-10.12, solutions to the equations were required over a range of input values of A for each of the two input values of H . If more H values were of interest, and if, for example, one wished to study the effect of varying λ_c and/or Δ , then the volume of computer output would quickly become massive and unwieldy. In general, insight into the environment generated by a class of fire

scenario (e.g., the semi-universal fire of Figure 3-10.11 in a room of arbitrary $H, A, \Delta, \lambda_r,$ and λ_c) is most clear when solutions can be obtained and displayed by means of limited numbers of graphs, charts, or tables. In this section, features of such a solution for an important, practical class of fire scenario will be displayed graphically, and explanation on how to extract practical results from this will be presented by way of examples. Some very useful and surprising time-of-smoke-filling estimates are obtained from this solution, and these will also be presented.

Q ∝ tⁿ Fire and Its Governing Equations

This subsection will present and solve Equations 9 through 11 and 25 for the broad class of fires whose $\dot{Q}(t)$ can be reasonably approximated by growth rates proportional to t^n for arbitrary $n \geq 0$ and whose product of combustion generation rates, $C(t)$, are approximately proportional to $\dot{Q}(t)$. This class of fire includes the constant fire, $n = 0$, and the t^2 growing fires, $n = 2$, both of which have been used in a variety of different references to describe the burning of many practical assemblies of combustibles. To be definite, it is assumed that Q and C can be approximated by

$$\dot{Q}(t) = \dot{Q}_0(tH^{3/2}g^{1/2}/A)^n; \quad C(t) = \beta Q(t) \quad (34)$$

where \dot{Q}_0 represents a characteristic energy release rate, n is any non-negative integer, and β is a constant of proportionality of appropriate dimension.

Notice that for the constant fire problem, $n = 0$ in Equation 34 and \dot{Q}_0 is simply the specified constant energy release rate of the fire. Also, the energy release rate in many practical fires is simulated by $n = 2$ -type fires and is approximated by⁴

$$\dot{Q}(t) = (1000/t_g^2)t^2 \text{ kW} \quad (35)$$

where t_g , the growth time of the fire, is defined as the time for the fire to grow in a t^2 -type manner from a small flaming fire to a fire of approximately 1000 kW. Equation 34 for $n = 2$ and Equation 35 lead to the result that for these "t-squared" fires, \dot{Q}_0 should be chosen as⁴

$$\dot{Q}_0 = [1000A^2/(t_g^2gH^3)] \text{ kW for } \dot{Q} \sim t^2 \text{ fires} \quad (36)$$

It is convenient to introduce the following dimensionless variables and parameters:

$$\left. \begin{aligned} \zeta &= Z_i/H \quad (\text{interface elevation}) \\ \phi &= T/T_a \quad (\text{upper layer temperature}) \\ \mu &= (1 - \lambda_c)M/(\beta C_p T_a) \\ &\quad (\text{upper layer product concentration}) \\ \tau &= 3[(1 - \lambda_r)Q_0^*]^{1/3}(tH^{3/2}g^{1/2}/A)^{(n+3)/3}/(n+3) \\ &\quad (\text{time}) \\ \epsilon &= (1 - \lambda_c)[(n+3)/3]^{2n(n+3)}Q_0^{*2/(n+3)}(1 - \lambda_r)^{(n+1)/(n+3)} \\ &\quad (\text{fire strength}) \\ \dot{Q}_0^* &= \dot{Q}_0/(\rho_a C_p T_a g^{1/2} H^{5/2}) \\ &\quad (\text{characteristic energy release rate}) \\ \delta &= \Delta/H \quad (\text{fire elevation}) \end{aligned} \right\} (37)$$

Using the above definitions in the model Equations 7, 9, 10, 13, and 16 through 18, eventually leads to the following equations for $\tau, \phi,$ and μ

$$\frac{d\zeta}{d\tau} = \begin{cases} -\epsilon\tau^{2n(n+3)} - 0.210\zeta^{5/3}, & 0 < \zeta \leq 1 \\ -\epsilon\tau^{2n(n+3)}, & -\delta < \zeta \leq 0 \\ 0; & \zeta = -\delta \end{cases} \quad (38)$$

$$\phi = \left\{ 1 - \frac{(n+3)\epsilon\tau^{3(n+1)/(n+3)}}{3(n+1)(1-\zeta)} \right\}^{-1}; \quad -\delta < \zeta \leq 1 \quad (39)$$

$$\frac{d\phi}{d\tau} = \frac{\epsilon\phi\tau^{2n/(n+3)}}{(1+\delta)}; \quad \zeta = -\delta$$

$$\mu = \phi - 1; \quad -\delta \leq \zeta \leq 1 \quad (40)$$

where Equation 38 must be solved subject to

$$\zeta(\tau = 0) = 1 \quad (41)$$

and where early time estimates for $\zeta, \phi,$ and μ are for $n = 0$:

$$\left. \begin{aligned} \lim_{\tau \rightarrow 0} (\zeta - 1)/(1 + \epsilon/0.210) \\ = -0.210\tau + \text{higher order terms in } \tau \\ \lim_{\tau \rightarrow 0} \phi/(1 + \epsilon/0.210) \\ = \lim_{\tau \rightarrow 0} (\mu + 1)/(1 + \epsilon/0.210) \\ = 1 + 5\epsilon\tau/6 + \text{higher order terms in } \tau \end{aligned} \right\} (42)$$

for $n > 0$:

$$\left. \begin{aligned} \lim_{\tau \rightarrow 0} (\zeta - 1) &= -0.210\tau + \text{higher order terms in } \tau \\ \lim_{\tau \rightarrow 0} (\phi - 1) &= \lim_{\tau \rightarrow 0} \mu \\ &= \frac{(n+3)\epsilon\tau^{2n/(n+3)}}{3(n+1)(0.210)} + \text{higher order terms in } \tau \end{aligned} \right\} (43)$$

Equation 38 describes the rate of descent of the interface as it passes through the regions above the fire ($0 < \zeta < 1$), below the fire ($-\delta < \zeta < 0$), and at the floor ($\zeta = -\delta$). Equations 39 and 40 describe the corresponding upper layer temperature and product concentration. Equations 42 and 43 are useful in starting a numerical solution to Equations 38 and 39.

Discussion of the Equations

The last subsection presented the equations which govern the dynamics of the interface, ζ , the upper layer temperature, ϕ , and the upper layer product concentration, μ . From Equation 40, the solution for μ would follow directly from the solution for ϕ . From the time of ignition to the time that the interface drops to the floor of the enclosure, a solution for ϕ could be obtained from Equations 39, 42, and 43, provided a solution for ζ was available. Beyond that time, the solution for ϕ could be determined by a direct integration of the second line of Equation 39.

With the above observations, attention is drawn to the solution for ζ . From ignition at $\tau = 0$ until $\tau = \tau_0 \equiv \tau(\zeta = 0)$, corresponding to the time when the interface drops to $\zeta = 0$, ζ is governed by Equation 41 and the first line of Equation 38. No general closed form solution is possible, and a numerical solution for $\zeta(\tau; \epsilon, n)$ is in order. Once this has been obtained, the solution can be extended beyond τ_0 by direct integration of the second and third lines of Equation 38.

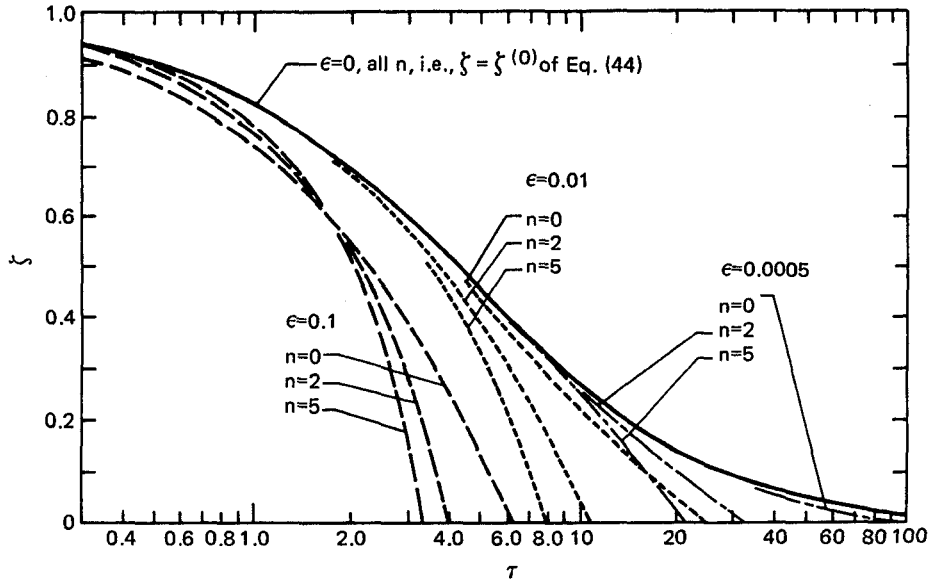


Fig. 3-10.18. Plots of $\zeta(\tau)$ for different values of n and ϵ , $0 < \tau \leq \tau_0$.

Solutions from Ignition to τ_0

In general, there is no particular problem in using a computer to integrate Equation 38 numerically and obtain ζ . However, in terms of generating a display of working graphical solutions which include times when ζ is small and positive, a problem does arise in the limit as ϵ approaches 0 (e.g., for small, dimensionless fire strength, Q^*). Applying such a limit to the first line of Equation 38 leads, in a first approximation, to the total neglect of the earlier referenced (left-hand) expansion term in comparison to the (right-hand) entrainment term. This corresponds, physically, to the situation of an interface that approaches the elevation of the fire, $\zeta = 0$, asymptotically in time. In the present nomenclature, and for a source whose strength grows as t^n , the solution for $\epsilon = 0$ is found to be

$$\zeta(\tau; \epsilon = 0, n) = \zeta^{(0)}(\tau) = [1 + 0.210(2/3)\tau]^{-3/2} \quad (44)$$

This result is plotted in Figure 3-10.18 along with numerically obtained, non-zero ϵ solutions for ζ .

From Equation 44 it is clear that for $\epsilon = 0$, $\zeta \rightarrow 0$ as $\tau \rightarrow \infty$. But, for a fixed n and an arbitrarily small but non-zero ϵ , a $\zeta = 0$ position of the interface will, in fact, be attained at some finite, large $\tau = \tau_0$.

This small ϵ behavior of ζ and its proximity to the $\epsilon = 0$ solution can be observed in Figure 3-10.18. As can be seen, the smaller the value of ϵ and the closer the value of n to 0, the longer in time the actual solution is accurately approximated by the $\epsilon = 0$ solution.

The small ϵ limit is very important in problems of physical interest. As an example, consider a constant ($n = 0$) smolder source of 0.5 kW, located a distance of 2 m below a ceiling with $\lambda_r = 0.1$ and $\lambda_c = 0.75$. This leads to $\epsilon = 5.3 (10^{-4})$. As an example of a relatively strong fire, consider a constant flaming fire of 5,000 kW (e.g., a burning gasoline spill approximately 1 m in radius) located 5 m below a ceiling, with $\lambda_r = 0.35$ and $\lambda_c = 0.75$. This leads to $\epsilon = 6.0 (10^{-2})$. In terms of a "small ϵ " criterion, the latter fire is still relatively weak.

Time, Temperature, and Concentration when the Smoke Drops to the Fire Elevation

Numerically computed τ_0, ϵ pairs were obtained and plotted by Cooper⁴³ for a variety of different n values. The corresponding values for $\phi_0 = \phi(\tau_0; \epsilon, n)$ were also obtained and plotted. All these results are reproduced here in Figure 3-10.19. From these plots and for arbitrary ϵ and n , it is possible to find the time, t_0 , which corresponds to τ_0 , for the smoke layer to drop to the fire elevation at $Z = 0$. The plots also provide an estimate for $\phi_0 = \phi(t_0)$, from which it is possible to obtain the $t = t_0$ upper layer temperature, T_0 , and (if applicable) the product of combustion concentration, M_0 . The most interesting general feature of Figure 3-10.19 is that, for a given n , the value of the ordinate

$$\epsilon^{2(n+3)/[3(n+5)]} \tau_0(\epsilon; n) = f(\epsilon; n) \quad (45)$$

is relatively uniform over a broad ϵ range of interest. For example, for $n = 0, 1$, and 2

$$\epsilon^{2/5} \tau_0(\epsilon; n = 0) = f(\epsilon; n = 0) = 4.3(1 \pm 0.15)$$

$$\epsilon^{1/3} \tau_0(\epsilon; n = 1) = f(\epsilon; n = 1) = 3.4(1 \pm 0.16) \quad (46)$$

$$\epsilon^{10/33} \tau_0(\epsilon; n = 2) = f(\epsilon; n = 2) = 3.0(1 \pm 0.17)$$

for ϵ in the range

$$0.2(10^{-4}) < \epsilon < 0.2(10^{-1}) \quad (47)$$

[With somewhat larger errors, Figure 3-10.19 indicates that estimates of τ_0 coming from Equation 46 would remain valid even for ϵ significantly smaller than $0.2(10^{-4})$.] This result can be expressed in practical terms as a general solution for t_0

$$t_0 = [f(\epsilon; n)]^{3/(n+3)} \left\{ \frac{[A(n+3)/3]^5 [\rho_a C_p T_a t_0^n / Q(t_0)]^3}{(1-\lambda_c)^2 (1-\lambda_r)g} \right\}^{1/(3n+5)} \quad (48)$$

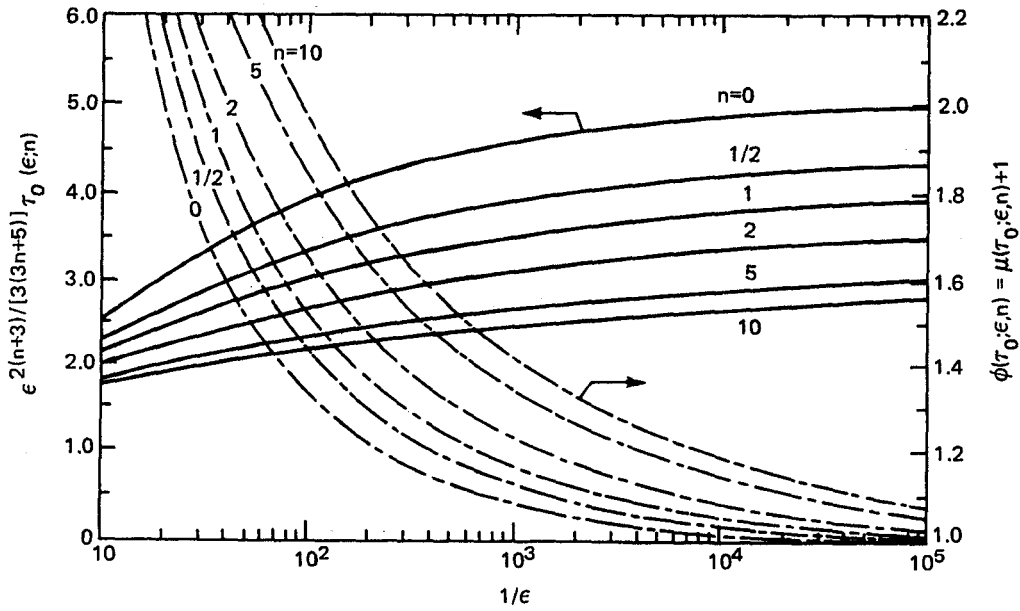


Fig. 3-10.19. Plots of $\epsilon^{2(n+3)/[3(3n+5)]}\tau_0$ and ϕ_0 as functions of $1/\epsilon$ for different values of n .

where the $f(\epsilon;n)$ are provided in Equation 46, or can be found from Figure 3-10.19. Also,

$$\epsilon = (1 - \lambda_c) \left\{ \frac{[A(n+3)/3]^{2n} [Q(t_0)/t_0^n]^2}{(1 - \lambda_r)^{(n+1)} (\rho_a C_p T_a)^2 g^{(n+1)} H^{(3n+5)}} \right\}^{1/(n+3)} \quad (49)$$

Thus, the analysis has led to a remarkable practical result, namely, for fires which grow at rates which are approximately proportional to t^n and for a wide range of fire elevations and room heights of practical interest, the time for a smoke layer to drop from the ceiling to the elevation of the fire is relatively independent of H .

Taking ρ_a , T_a , C_p , and g to be

$$\begin{aligned} \rho_a &= 1.18 \text{ kg/m}^3, \quad T_a = 294 \text{ K}, \quad g = 9.8 \text{ m/s}^2. \\ C_p &= 240 \text{ cal/(kgK)} = 1.005 \text{ Ws/m}^3 \end{aligned} \quad (50)$$

Equations 48 and 49 for $n = 0, 1$, and 2 become

$n = 0$:

$$\begin{aligned} t_0 &= 91.4(1 \pm 0.15) [A/Q^{3/5}] / [(1 - \lambda_c)^2 (1 - \lambda_r)]^{1/5} \\ \epsilon &= 9.43(10^{-3}) (Q^2/H^5)^{1/3} (1 - \lambda_c) / (1 - \lambda_r)^{1/3} \end{aligned} \quad (51)$$

(A in m^2 , Q in kW , t_0 in sec , H in m)

$n = 1$:

$$\begin{aligned} t_0 &= 20.2(1 \pm 0.12) \{A^5 [t_0/Q(t_0)]^3 / [(1 - \lambda_c)^2 (1 - \lambda_r)]\}^{1/8} \\ \epsilon &= 1.98(10^{-2}) \{A [Q(t_0)/t_0] / (1 - \lambda_r)\}^{1/2} (1 - \lambda_c) / H^2 \end{aligned} \quad (52)$$

(A in m^2 , Q in kW , t_0 in sec , H in m)

$n = 2$:

$$\begin{aligned} t_0 &= 10.5(1 \pm 0.10) \{A^5 [t_0^2/Q(t_0)]^3 / [(1 - \lambda_c)^2 (1 - \lambda_r)]\}^{1/11} \\ \epsilon &= 3.68(10^{-2}) (1 - \lambda_c) \{A^4 [Q(t_0)/t_0^2] / [H^{11} (1 - \lambda_r)^3]\}^{1/5} \end{aligned} \quad (53)$$

(A in m^2 , Q in kW , t_0 in sec , H in m)

or, in terms of t_g of Equation 35,⁴

$n = 2$:

$$\begin{aligned} t_0 &= 1.60(1 \pm 0.10) \{A^5 t_g^6 / [(1 - \lambda_c)^2 (1 - \lambda_r)]\}^{1/11} \\ \epsilon &= 0.583(1 - \lambda_c) \{A/t_g\}^4 / [H^{11} (1 - \lambda_r)^3]\}^{1/5} \end{aligned} \quad (54)$$

(A in m^2 , Q in kW , t_0 and t_g in sec , H in m)

where all the above t_0 estimates are subject to the ϵ range of Equation 47.

Some Solution Results for $Z_i(t)$, $T(t)$, and $\mu(t)$

Plots of general solutions for $Z_i(t)$, $T(t)$, and $\mu(t)$ are presented in Figure 3-10.20 for $n = 0, 1$, and 2 . These plots are useful up to the times when the interface either drops to the floor of the compartment or to an elevation $0.2 H$ below the fire, whichever event occurs first.

As can be noted, the abscissa of the Figure 3-10.20 plots, which have been taken from Cooper,⁴³ are in the form

$$\sigma = \{\text{constant}\} t^{\sigma+1}$$

The σ of Figure 3-10.20 corresponds to

$$\sigma = \{(n+3)/[3(n+1)]\} \epsilon \tau^{3(n+1)/(n+3)} \quad (55)$$

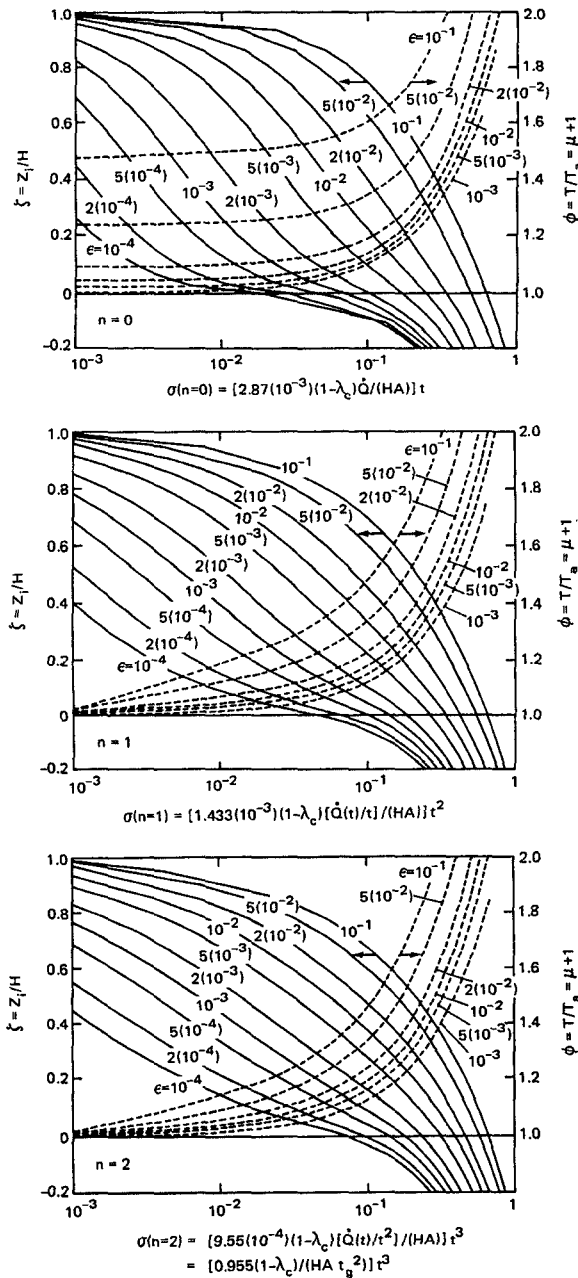


Fig. 3-10.20. Plots of $Z_i(t)$, $T(t)$, and $\mu(t)$ up to the time when $Z_i = -0.2 H$ or $Z_i = Z_{\text{floor}}$, whichever comes first, for different values of ϵ and for $n = 0, 1$, and 2 . (\dot{Q} in kW; t and t_g in s; H in m; and A in m^2 .)

under the ambient property assumptions of Equation 50. Cooper found σ to be a convenient variable for describing the upper layer environment after the interface had dropped below the fire elevation, $Z_i = 0$, and even subsequent to the time that the interface drops to the compartment floor, i.e., when $Z_i = -\Delta$.⁴³ A description of solutions to our problem at these latter times is beyond the scope of this chapter, and the reader is referred to Cooper's work for a full discussion of the relevant results.⁴³

USING THE $\dot{Q} \sim t^n$ SOLUTION PLOTS OF FIGURES 3-10.19 AND 3-10.20 TO PREDICT CHARACTERISTICS OF COMPARTMENT FIRE-GENERATED ENVIRONMENTS

To illustrate the use of the solution plots of Figures 3-10.19 and 3-10.20, they will now be applied to two example problems. The first example will involve a problem of smoldering combustion. The second example illustrates the use of the theory in predicting the environment produced in an enclosure which contains a specific large-scale flaming fire hazard.

EXAMPLE 1:

Smoldering combustion: Smoldering experiments reported by Quintiere *et al* were carried out in a single-room compartment of height 2.44 m and floor area 8.83 m^2 .⁴⁵ The opening to the enclosure was formed by a closed undercut door, where the undercut formed a 0.76 m \times 0.025 m open horizontal slit at floor level. A smoldering ignition source was placed in the enclosure with the top surface of the source at an elevation of 0.33 m. Gas analysis was carried out at four equidistant elevations, the inlets of sampling tubes extending horizontally approximately 0.5 m from the walls.

The tests evaluated two different smolder sources: a loosely packed bed of cotton, and blocks of flexible polyurethane foam. Mass loss rates, \dot{m} , were found to be approximately linear in time throughout the first hour of the two tests, i.e.,

$$\dot{m} = \alpha t \quad 0 < t < 60 \text{ min} \quad (56)$$

where

$$\alpha = \begin{cases} 0.21 \text{ g/min}^2 & \text{for polyurethane} \\ 0.33 \text{ g/min}^2 & \text{for cotton} \end{cases}$$

The heats of combustion, H_c , of the materials as well as the ratios, γ , of mass-of-CO produced to mass of material lost were obtained in a separate small-scale apparatus. These were found to be

$$H_c = \begin{cases} (11 \pm 1) \text{ kJ/g}_{\text{cotton}} \\ (15 \pm 8) \text{ kJ/g}_{\text{polyurethane}} \end{cases} \quad (57)$$

$$\gamma = \begin{cases} 0.11 \text{ g}_{\text{CO}}/\text{g}_{\text{cotton}} \\ (0.10 \pm 0.01) \text{ g}_{\text{CO}}/\text{g}_{\text{polyurethane}} \\ (0.10 \pm 0.04) \text{ g}_{\text{CO}}/\text{g}_{\text{polyurethane}} \end{cases} \quad (58)$$

The results of the previous section will be used to predict the environment which developed in the enclosure during the course of the two different material evaluations.

Comparing Equations 56 through 58 to Equation 34 leads to

$$\begin{aligned} \dot{Q} &= \alpha H_c t = \dot{Q}_0 [t H_c^3 / 2 g^{1/2} / A]^n \\ \dot{C}_{\text{CO}} &= \alpha \gamma t = \beta \dot{Q} \end{aligned} \quad (59)$$

where \dot{C}_{CO} is measured in g_{CO} per unit time. From the above, it is concluded that

$$n = 1; \quad Q(t)/t = \alpha H_c; \quad \beta = \gamma/H_c \quad (60)$$

Also

$$H = 2.11 \text{ m}, \Delta = 0.33 \text{ m}, A = 8.83 \text{ m}^2 \quad (61)$$

Radiant losses from the combustion zone are neglected, i.e., $\lambda_r = 0$. Considerations by Cooper,⁴⁰ together with the experimental results of Mulholland *et al* and Veldman *et al*,^{46,13} indicate that for a $\lambda_r = 0$ combustion zone in an enclosure with proportions similar to the present one, $\lambda_c \approx 0.6$. This λ_c will be used here.

Using the λ_c value 0.6 and Equations 50, 57, 58, and 60 in the μ definition of Equation 37 and the result of Equation 40 leads to

$$\phi = 1 + 135M_{cotton} = 1 + 204M_{polyurethane} \quad (62)$$

where, e.g., M_{cotton} is the upper layer concentration of CO ($g_{CO}/g_{upper \text{ layer}}$) during smoldering of the cotton source. From Equations 56 and 57

$$\frac{Q(t)}{t} = \alpha H_c \approx \begin{cases} 0.21(15) \text{ kJ/min}^2 = 9(10^{-4}) \text{ kW/s for polyurethane} \\ 0.33(11) \text{ kJ/min}^2 = 9(10^{-4}) \text{ kW/s for cotton} \end{cases} \quad (63)$$

All parameters of the problem required to estimate t_0 and ϵ from Equation 52 are now available. These are found to be

$$t_0 = 1400 \text{ sec}; \quad \epsilon = 1.6(10^{-4}) \quad (64)$$

The value of ϵ satisfies the ϵ range of Equation 47 thereby establishing the validity of the t_0 estimate.

From the value of ϵ , it is now possible to use Figure 3-10.19 to obtain ϕ_0 . Thus, for $1/\epsilon = 0.61(10^4)$ and for $n = 1$ it is found from the Equation 37 definition of ϕ that

$$\phi_0 = 1.07 \rightarrow T(t_0) = 1.07T_a = 315 \text{ K} = 42^\circ\text{C} \quad (65)$$

Also, from Equation 62, this result for ϕ_0 yields

$$\left. \begin{aligned} M_{cotton}(t_0) &= (1.07 - 1)/135 \\ &= 5(10^{-4})g_{CO}/g_{upper \text{ layer}} \\ &= 5(10^2) \text{ ppm CO} \\ M_{polyurethane}(t_0) &= (1.07 - 1)/204 \\ &= 3(10^{-4})g_{CO}/g_{upper \text{ layer}} \\ &= 3(10^2) \text{ ppm CO} \end{aligned} \right\} \quad (66)$$

The smoke interface reaches the floor at the time, t_f , corresponding to

$$\zeta_f = Z_i(t_f)/H = -\Delta/H = \delta = -0.16 \quad (67)$$

From the $n = 1$ plots of Figure 3-10.20, it is found that this occurs at t_f corresponding to

$$\begin{aligned} \sigma = 0.3 &= \sigma_f(\zeta = \zeta_f, n = 1) \\ &= \{1.4(10^{-3})(1 - \lambda_c)[\dot{Q}(t)/t]/(HA)\}t_f^2 \\ &\quad (\dot{Q} \text{ in kW}; t \text{ in s}; H \text{ in m}; A \text{ in m}^2) \\ &= \{1.4(10^{-3})(1 - 0.6)[9(10^{-4})]/[(2.1)(8.8)]\}t_f^2 = 0.3(10^{-7})t_f^2 \end{aligned} \quad (68)$$

(for both the cotton and polyurethane) at which time

$$\phi(t_f) = \phi_f \approx 1.25 \quad (69)$$

The following results are obtained from Equations 68 and 69 and with the use of Equation 62.

$$t_f = 3(10^3) \text{ sec}$$

$$M_{cotton}(t_f) = (1.25 - 1)/135 = 1.9(10^3) \text{ ppm CO} \quad (70)$$

$$M_{polyurethane}(t_f) = (1.25 - 1)/204 = 1.2(10^3) \text{ ppm CO}$$

Thus, the above estimate indicates that the interface reached the floor elevation somewhat prior to the 60-min duration of the tests. The reader is referred to Cooper's studies for further discussion of comparisons between calculated and experimental results.⁴³

EXAMPLE 2:

Hazard development in enclosures containing some larger scale fires: NFPA 204M, *Guide for Smoke and Heat Venting*, provides a catalogue of experimentally determined energy release rates for the growth stages of flaming fires in practical fuel assemblies.⁴ The \dot{Q} of all items in this listing is proportional to t^2 . For example, the \dot{Q} of many items can be estimated by

$$\dot{Q} = 0.10t^2 \text{ kW/s}^2 \quad (71)$$

Using Equation 35, this corresponds to

$$\dot{Q} = 0.10t^2 \text{ kW/s}^2 \quad (72)$$

The latter items include wood pallets stacked 3.0 to 4.6 m high, many different types of polyethylene, polypropylene, polystyrene and PVC commodities in cartons stacked 4.6 m high, and a horizontal polyurethane mattress.

The results of Figures 3-10.19 and 3-10.20 will be used to characterize the hazard development in enclosures which contain Equation 71-type fires.

From Equations 54 and 71 and the abscissa for $n = 2$ of Figure 3-10.20

$$\begin{aligned} t_0 &\approx 20 \cdot \{A^5/[(1 - \lambda_c)^2(1 - \lambda_r)]\}^{1/11} \\ \epsilon &= 1.5(10^{-2})\{1 - \lambda_c\}A^{4/5}/\{[1 - \lambda_r]^{3/5}H^{11/5}\} \\ \sigma(n = 2) &= 0.96(10^{-4})\{[1 - \lambda_c]/(HA)\}t^3 \end{aligned} \quad (73)$$

(t in sec; H in m; A in m^2)

With Equation 73, Figures 3-10.19 and 3-10.20 can now be used to answer a wide variety of hazard-related questions. For illustrative purposes, two such questions will be addressed here.

QUESTION 1:

Flaming ignition is initiated in stacked commodities of the "tg = 100 s variety" which are contained in a warehouse of height 6 m and floor area 1500 m^2 . At what time does the upper layer attain the potentially untenable temperature (due to downward radiation) of 183°C, and what is the elevation of the layer interface at this time?¹ At what time does the upper layer completely fill the warehouse?

ANSWER:

Consistent with recommendations by Cooper,² assume $\lambda_r = 0.35$, and, for the purpose of a hazard analysis of this

type, conservatively assume that $\lambda_c = 0.6$. Take H to be the floor-to-ceiling dimension, 6 m, and Δ to be zero. Then, for $A = 1500 \text{ m}^2$, Equation 73 leads to

$$\begin{aligned} t_0 &= 680 \text{ sec} \\ \varepsilon &= 5.2(10^{-2}) \\ \sigma(n=2) &= 4.7(10^{-9})t^3 \end{aligned} \quad (74)$$

Notice that the above value for $\varepsilon = 5.2(10^{-2}) > 0.2(10^{-1})$ is somewhat outside the Equation 47 range. As a result, the above $t_0 = 680 \text{ s}$ estimate is not reliable. A better value for t_0 , estimated from Equation 48 and Figure 3-10.19, is found to be $t_0 \approx 600 \text{ s}$.

The $\varepsilon = 5.2(10^{-2})$ value corresponds to $1/\varepsilon = 19$ which, for $n = 2$ in Figure 3-10.19, is found to correspond (somewhat off-scale) to

$$\phi_0 \approx 2.4 \rightarrow T(t_0) = 2.4T_a = 710 \text{ K} = 433^\circ\text{C} \quad (75)$$

At the time, t_u , of potential untenability, $T_u = T(t_u)$ is assumed to be 183°C (456 K). Thus

$$\phi_u = \phi(t_u) = T_u/T_a = 456/294 = 1.55 \quad (76)$$

For $\varepsilon = 5.2(10^{-2})$, the $n = 2$ plots of Figure 3-10.20 can be interpolated at $\phi = \phi_u = 1.55$ to yield

$$\sigma_u = \sigma(t_u) \approx 0.2 = 4.7(10^{-9})t_u^3 \rightarrow t_u = 350 \text{ sec} \quad (77)$$

which, in turn, is seen to correspond to

$$\zeta_u = \zeta(t_u) = Z_i(t_u)/H = 0.45 \quad (78)$$

Using this last value for ζ_u along with $H = 6 \text{ m}$ leads to

$$Z_i(t_u) = 0.45(6) \text{ m} = 2.7 \text{ m} \quad (79)$$

The above results are summarized as follows: the upper smoke layer will fill the compartment at $t_0 = 600 \text{ s}$, at which time its average temperature will be approximately 430°C . The potentially untenable condition of $T = 183^\circ\text{C}$ will occur at $t_u = 350 \text{ s}$, at which time the layer interface is 2.7 m above the floor.

QUESTION 2:

Flaming ignition is initiated in a polyurethane mattress 0.6 m above the floor of a hospital ward with floor-to-ceiling dimension of 3 m and floor area 100 m^2 . At what time, t_u , does the upper layer interface reach the potentially untenable elevation, $Z_u = 1.5 \text{ m}$, and what is the upper layer temperature, T_u , at this time?

ANSWER:

Take $\lambda_c = 0.8$, and $\lambda_r = 0.35$. Also, $H = 2.4 \text{ m}$, $\Delta = 0.6 \text{ m}$, $Z_u = 0.9 \text{ m}$, and $A = 100 \text{ m}^2$. Then, Equation 73 leads to

$$\begin{aligned} t_0 &= 230 \text{ sec} \\ \varepsilon &= 2.3(10^{-2}) \\ \sigma(n=2) &= 8.0(10^{-8})t^3 \end{aligned} \quad (80)$$

Also, at the time of untenability

$$Z_i(t_u)H = Z_u/H = 0.9/2.4 = 0.38 \quad (81)$$

For $\varepsilon = 2.3(10^{-2})$, the $n = 2$ plots of Figure 3-10.20 can be interpolated to obtain the desired values of $\sigma(t_u)$, and then $\phi(t_u)$ corresponding to $Z_i/H = 0.38$. Thus

$$\begin{aligned} \sigma(t_u) &= 0.18 = 80(10^{-9})t_u^3 \rightarrow t_u = 130 \text{ sec} \\ \phi(t_u) &= 1.33 \rightarrow T(t_u) = 1.33T_a = 391 \text{ K} = 118^\circ\text{C} \end{aligned} \quad (82)$$

In Equation 80, t_0 is the time for the smoke interface to drop to the level of the mattress which is 0.6 m above the floor. As an additional point of information, for $\varepsilon = 2.3(10^{-2})$, corresponding to $1/\varepsilon = 44$, and for $n = 2$, Figure 3-10.19 provides the result

$$\phi_0 = 1.94 \rightarrow T(t_0) = 1.94T_a = 570 \text{ K} = 297^\circ\text{C} \quad (83)$$

Notice that this result can also be obtained approximately from Figure 3-10.20. To do so, select the value of $\sigma = \sigma(t_0)$ when $\zeta = Z_i/H = 0$, and find the corresponding value for $\phi = \phi(t_0)$, all on the $\varepsilon = 2(10^{-2})$ curves. This leads to $\phi(t_0) = 1.88 \approx 1.94$.

The above results are summarized as follows: the smoke layer interface will drop to the 1.5-m elevation at $t = 130 \text{ s}$, at which time its average temperature will be approximately 118°C . Also, the interface will reach the mattress elevation at $t = 230 \text{ s}$ and have an average temperature of 297°C .

REFERENCES CITED

1. L.Y. Cooper, "A Concept for Estimating Available Safe Egress Time in Fires," *F. Safety J.*, 5, pp. 135-144 (1983).
2. L.Y. Cooper, "A Mathematical Model for Estimating Available Safe Egress Time in Fires," *F. and Mats.*, 6, pp. 135-144 (1982).
3. E.G. Butcher and A.C. Parnell, *Smoke Control and Fire Safety Design*, Spon, London (1979).
4. G. Heskestad, "Appendix A," NFPA 204M, *Guide for Smoke and Heat Venting*, National Fire Protection Association, Quincy (1991).
5. V. Babrauskas, "Combustion of Mattresses Exposed to Flaming Ignition Sources, Part I, Full-Scale Tests and Hazard Analysis," *NBSIR 77-1290*, National Bureau of Standards, Gaithersburg (1977).
6. G. Heskestad, "Engineering Relations for Fire Plumes," *F. Safety J.*, 7, pp. 25-32 (1984).
7. E.E. Zukoski, T. Kubota, and B. Cetegen, "Entrainment in Fire Plumes," *F. Safety J.*, 3, pp. 107-121 (1980/81).
8. B.J. McCaffrey, "Purely Buoyant Diffusion Flames: Some Experimental Results," *NBSIR 79-1910*, National Bureau of Standards, Gaithersburg (1979).
9. R.L. Alpert, "Turbulent Ceiling-Jet Induced by Large-Scale Fires," *Comb. Science Tech.*, 11, pp. 197-213 (1975).
10. G. Heskestad, "Similarity Relations for the Initial Convective Flow Generated by Fire," *Paper 72-WA/HT-17*, Winter Annual Meeting, ASME (1972).
11. G. Heskestad and M.A. Delichatsios, "Environments of Fire Detectors—I: Effect of Fire Size, Ceiling Heights, and Material," Vol 1: Measurements, *FMRC Report NBS-GCR-77-86*, Vol. 2: "Analysis," *FMRC Report NBS-GCR-77-95*, National Bureau of Standards, Gaithersburg (1977).
12. G. Heskestad and M.A. Delichatsios, "Environments of Fire Detectors—II: Effect of Ceiling Configuration," Vol 1: Measurements, *FMRC Report NBS-GCR-78-128*, Vol. 2: "Analysis," *FMRC Report NBS-GCR-78-129*, National Bureau of Standards, Gaithersburg (1978).
13. C.C. Veldman, T. Kubota, and E.E. Zukoski, "An Experimental Investigation of Heat Transfer from a Buoyant Plume to a Horizontal Ceiling—Part I: Unobstructed Ceiling," *C.I.T. Report NBS-GCR-77-97*, National Bureau of Standards, Gaithersburg (1975).

14. L.Y. Cooper, "Heat Transfer from a Buoyant Plume to an Unconfined Ceiling," *J. of Heat Transfer*, 104, pp. 446-451 (1982).
15. L.Y. Cooper and A. Woodhouse, "The Buoyant Plume-Driven Adiabatic Ceiling Temperature Revisited," *J. of Heat Transfer*, 108, pp. 822-826 (1986).
16. L.Y. Cooper and D.W. Stroup, "The Thermal Response of Unconfined Ceilings Above Growing Fires and the Importance of Convective Heat Transfer," *J. of Heat Transfer*, 109, pp. 172-178 (1987).
17. R.L. Alpert, "Calculation of Response Time of Ceiling Mounted Fire Detectors," *Fire Tech.*, 3, pp. 181-195 (1972).
18. I. Benjamin, G. Heskestad, R. Bright, and T. Mayes, *An Analysis of the Report on Environments of Fire Detectors*, Fire Detection Institute (1979).
19. D. Goldman and Y. Jaluria, "Effect of Opposing Buoyancy on the Flow in Free and Wall Jets," *J. of Fluid Mech.*, 166, pp. 41-56 (1986).
20. L.Y. Cooper, "Ceiling Jet Properties and Wall Heat Transfer Near Regions of Ceiling Jet-Wall Impingement," *NBSIR 86-3307*, National Bureau of Standards, Gaithersburg (1986).
21. L.Y. Cooper, "Convective Heat Transfer to Ceilings Above Enclosure Fires," *Proceedings of 19th Symposium (International) on Combustion*, Combustion Institute, Haifa (1982).
22. L.Y. Cooper, "A Buoyant Source in the Lower of Two, Homogeneous, Stably Stratified Layers—A Problem of Fire in an Enclosure," *Proceedings of 20th Symposium (International) on Combustion*, Combustion Institute, Pittsburgh, pp. 1567-1573 (1984).
23. L.Y. Cooper, "On the Significance of a Wall Effect in Enclosures with Growing Fires," *Comb. Science Tech.*, 40, pp. 19-39 (1984).
24. L.Y. Cooper and D.W. Stroup, "Calculating Available Safe Egress Time (ASET)—A Computer Program and User's Guide," *NBSIR 82-2578*, National Bureau of Standards, (1982). Also, a condensed version: "ASET—A Computer Program for Calculating Available Safe Egress Time," *F. Safety Jour.*, 9, pp. 29-45 (1985).
25. E.E. Zukoski and T. Kubota, "Two-Layer Modeling of Smoke Movement in Building Fires," *F. and Matls.*, 4, 1, pp. 17-27 (1980).
26. K. Steckler, J. Quintiere, and W. Rinkinen, "Flow Induced by Fire in a Compartment," *Proceedings of 19th Symposium (International) on Combustion*, Combustion Institute, Pittsburgh (1982).
27. NFPA 101, *Life Safety Code*, (A-15-3.1.3), National Fire Protection Association, Quincy (1994).
28. L.Y. Cooper, M. Harkelroad, J. Quintiere, and W. Rinkinen, "An Experimental Study of Upper Hot Layer Stratification in Full-Scale Multiroom Fire Scenarios," *J. of Heat Transfer*, 104, pp. 741-749 (1982).
29. L.Y. Cooper, "The Need and Availability of Test Methods for Measuring the Smoke Leakage Characteristics of Door Assemblies," *Fire Safety: Science and Engineering*, ASTM STP 882, ASTM, Philadelphia, pp. 310-329 (1985).
30. T. Wakamatsu, "Calculation of Smoke Movement in Buildings," *Res. Paper 34*, Building Research Institute, Tokyo (1968).
31. E. Evers and A. Waterhouse, "A Computer Model for Analyzing Smoke Movement in Buildings," *SCS Ltd. Report CP 68/78* for Fire Research Station, Borehamwood (1978).
32. B.R. Morton, G.I. Taylor, and J.S. Turner, "Turbulent Gravitational Convection from Maintained and Instantaneous Sources," *Proceedings of Royal Society (London)*, Ser. A, 234, pp. 1-23 (1956).
33. S. Yokoi, "On the Heights of Flames from Burning Cribs," *BRI Report 12*, Ministry of Construction, Japanese Government (1963).
34. W.D. Baines and J.S. Turner, "Turbulent Buoyant Convection from a Source in a Confined Region," *J. of Fluid Mech.*, 37, Part 1, pp. 51-80 (1969).
35. E.E. Zukoski, "Development of a Stratified Ceiling Layer in the Early Stages of a Closed-Room Fire," *F. and Matls.*, 2, pp. 54-62 (1978).
36. W.D. Walton, "ASET-B: A Room Fire Program for Personal Computers," *NBSIR 85-3144-1*, National Bureau of Standards, Gaithersburg (1985).
37. D. Burgess and M. Hertzberg, "Radiation from Pool Fires" in *Heat Transfer in Flames*, ed. by N.H. Afgan and J.M. Beer, Chap. 27, Wiley and Sons, New York (1974).
38. J. DeRis, "Fire Radiation—A Review," *Tech. Report FMRC RC 78-BT-27*, Factory Mutual Research Corp., Norwood (1978).
39. A.T. Modok and P.A. Croce, "Plastic Pool Fires," *Comb. Flame*, 30 (1977).
40. L.Y. Cooper, "Estimating Safe Available Egress Time from Fires," *NBSIR 80-2172*, National Bureau of Standards, Gaithersburg (1981).
41. R. Friedman, "Quantification of Threat from a Rapidly Growing Fire in Terms of Relative Material Properties," *F. and Matls.*, 2, pp. 27-33 (1978).
42. T. Tanaka, "A Model on Fire Spread in Small-Scale Building," *Third Joint Meeting US-Japan Panel on Fire Research and Safety*, UJNR, Washington (1978).
43. L.Y. Cooper, "The Development of Hazardous Conditions in Enclosures with Growing Fires," *Comb. Science and Tech.*, 22, pp. 279-297 (1983).
44. J.G. O'Neill and W.D. Hayes, "Full-Scale Fire Tests with Automatic Sprinklers in a Patient Room," *NBSIR 79-1749*, National Bureau of Standards, Gaithersburg (1979).
45. J. Quintiere, M. Birky, and G. Smith, "An Analysis of Smoldering Fires in Closed Compartments and Their Hazard Due to Carbon Monoxide," *F. and Matls.*, 6, p. 99 (1982).
46. G. Mulholland, T. Handa, O. Sugawa, and H. Yamamoto, "Smoke Filling in an Enclosure," *20th National Heat Transfer Conference*, Milwaukee (1981).